TARGETED STEEL FRAMES BY MEANS OF INNOVATIVE MOMENT RESISTING CONNECTIONS

Salvatore Benfratello[1], Salvatore Caddemi[2], Luigi Palizzolo[1], Bartolomeo Pantò[3], Davide Rapicavoli[2] and Santo Vazzano[1]

[1] Department of Engineering, University of Palermo
Viale delle Scienze - 90128, Palermo, Italy
e-mail: salvatore.benfratello@unipa.it, luigi.palizzolo@unipa.it, santo.vazzano@unipa.it

[2] DICAR, University of Catania
Via Santa Sofia, 64 − 95123 Catania, Italy
scaddemi@dica.unict.it, drapicavoli@dica.unict.it

[3] Department of Civil and Environmental Engineering, Imperial College London
South Kensington Campus, London SW7 2AZ, United Kingdom, b.panto@imperial.ac.uk

Keywords: *FSDB* model, distributed plasticity, steel frames, innovative *RBS* connections, minimum volume design.

Abstract. *The present paper proposes the use of stepped cross section devices on steel frames aiming at reproducing a pre-established target push-over curve. To this aim a Limited Resistance Plastic Device (LRPD) to be inserted along selected structural members is proposed. The following two main specific features for LRPD are required: any elastic flexural stiffness variation of the original selected member must be avoided; an ultimate plastic bending moment value equal to an assigned percentage of the original limit resistance value must be ensured. Steel frames equipped with LRPD are modelled by means of an extension of a recently proposed Fibre Smart Displacement Based (FSDB) beam element model, characterized by the adoption of updating shape functions. The novelty of this research, with respect to previous studies, regards: i) the formulation of a targeted plane steel frame by means of a new optimal design procedure for the LRPD with assigned stiffness and resistance features, independent of each other; ii) the development of a FSDB beam element approach suitably devoted to such a special application of discontinuous cross sections devices. The design procedure and the FSDB model for the analysis of the real behaviour of the proposed LRPD device in the field of distributed plasticity is validated against detailed 3D finite element models.*

1 INTRODUCTION

Since more than a century, frame structures represent the more adopted structural typology both in civil and industrial constructions. Among these typologies, steel structures are certainly the more endorsed ones in terms of strength, weight, durability, construction speediness, space usability, material quality and behaviour flexibility.

Clearly, the response of a steel frame structure strongly depends on both the geometric characteristics of the structural elements and on the mechanical characteristics of the material. Moreover, the role played by the connection typology between the structural elements on the performance of a frame structure is equally decisive.

Usually, in frame structures, columns are continuous elements, and the potential connections are designed so as to guarantee the complete transmission of all the stresses between adjacent elements. On the other hand, the principal typologies of connections usually adopted between columns and beams are hinges located at the ends of the beams or internal clamped joints. Both typologies always guarantee the mechanical continuity but, in the case of hinges, beams are substantially designed to undergo the vertical actions to be transmitted to the columns, providing a very low contribution to the overall structural strength with respect to horizontal actions. Indeed, in the case of internal clamped joints, beams actively contribute to the overall strength with respect to horizontal actions, setting up a structure mechanically stronger and less deformable. In this last case of moment resisting connections, both the elastic behaviour of the relevant frame in terms of stiffness and the limit one in terms of collapse load just depend on the chosen cross section beam elements. Sometimes, the elastic behaviour and the limit resistance must be conveniently kept independent of each other.

In some recent papers ([1]-[6]), some of the authors proposed an innovative device devoted to realizing a new kind of moment resisting connection for steel elements referred to as Limited Resistance Rigid Perfectly Plastic Hinge (*LRPH*). The following main ideas constitute the backbone of *LRPH*:

i) create a preset zone of the beam in which plastic deformations develop, leaving the remaining part of the beam in the elastic range;

ii) design the device such that its flexural stiffness and resistance can be suitably assigned remaining independent of each other.

The use of such new devices allows to control the overall structural behaviour features of the frame in which they are inserted. Precisely, by exploiting the possibility of designing devices with stiffness and strength independent of each other, a targeted steel frame characterized by assigned capacity curves can be realized. This aspect is particularly considerable in the case of a frame conceived to substitute a portion of a masonry wall whose target is exhibiting a behaviour as close as possible to the replaced structure.

The proposed device, from a general point of view, can be framed into the so-called Reduced Beam Section (*RBS*) connections, but it possesses some further special features that make the device more widely usable, as it will be described in the following.

The main idea of *RBS* configuration is to cut portion of beam flanges near beam-to-column joint to form a suitable plastic hinge away from the joint for suitably reduced acting stress values.

In the framework of such equipment the so-called dog-bone sections play a particularly important role being the first typology proposed within the Reduced Beam Section (*RBS*) connections. The starting idea was suggested by Plumier in 1990 (see, e.g., [7]-[8]) and consists in cutting the flanges of the I-shape beam cross section at an assigned small distance from the column so that a plastic hinge can occur outside the beam-column connection with the further advantage of also reducing the acting moment within the connection. Successively, many configurations of cut profile have been proposed in both experimental and theoretical papers (see, e.g., [9]-[15]) and the related performance has been studied. Furthermore, some current codes [16, 17] report the guidelines for correctly designing the *RBS* connections.

The main advantages of *RBS* connections are related to the protection of the welded cross section between beam and column, to the increasing of the total energy dissipation and to the high rotational capacity of the portion interested by the flange cutting. The main drawbacks are represented by the local stiffness decrease, the reduced lateral strength and the risk of web buckling. In all the referenced papers, the model utilized to describe the behaviour of the *RBS* connections is the plastic hinge belonging to the concentrated plasticity approach.

The innovative device proposed by the authors is defined as a steel element characterized by symmetry with respect to three orthogonal barycentric planes and constituted by a sequence of three portions with abrupt cross section changes, each of one identifies a steel element of suitably designed geometry. In particular, the central inner portion is designed to represent the location where plastic deformations arise. The mechanical model so far adopted for *LRPH* has been characterized as a rigid perfectly plastic hinge. On the other hand, as proved in [21] and briefly reported also in the present paper, in order to ensure the complete plasticization of the inner portion cross section, the *LRPH* device must possess an adequate and non-negligible length. In the latter sense, the *LRPH* can be more appropriately considered as an additional special beam element. The non-negligible length implies the removal the initial and simplified rigid perfectly plastic hinge model adopted so far for the *LRPH* and to consider the real distribution of the plastic deformations occurring in the device element.

The latter evidence led the authors to propose in the present work a new definition of a special steel element aiming at improving the behaviour of such *LRPH* connections by accounting for a proper distributed plasticity diffusion along its length. The latter proposal will be referred to as Limited Resistance Plastic Device (*LRPD*). Furthermore, a new improved optimal design problem formulation for the device, taking into account the actual expected stress distribution on the entire element and introducing suitable new constraints on the imposed limit behaviour adopting a suitable energy formulation, is proposed.

The proposed *LRPD*, aiming at improving the mechanical behavior of such devices, requires suitable and specialized analytical modeling. To this aim, the present study is also devoted to formulating a new discontinuous beam finite element suitable to model the proposed *LRPD* able to provide accurate nonlinear analysis by avoiding any cumbersome mesh refinement usually required by standard beam elements at the onset of plastic deformations.

Development of plastic deformations is classically described by means of a distributed plasticity approach able to model diffusion of plasticity along a beam portion as well as along the cross-section height. Diffusion of plastic deformations along the beam axis can be followed

within the Finite Element Model (FEM) by means of the integration of the nonlinear plastic constitutive equations at pre-established Gauss integration cross sections [18]-[22]. Development of plastic deformation along the cross-section height can be described by performing a refined discretisation of the Gauss cross sections into cells or strips denoted as fibre approach [23]-[27]. Within the context of the FEM based on the formulation of shape functions of the displacement field, some of the authors recently proposed a Smart Displacement Based (*SDB*) beam element, with uniform cross section, endowed with adaptive displacement shape functions able to update during the inelastic analysis [28]. The term "smart" aims at emphasizing the ability of the element to upgrade the displacement shape functions according to the current inelastic state. The latter are hence also addressed to as "smart displacement shape functions".

The advantage of such beam element consists in avoiding any FE mesh or Gauss point refinement during the analysis. The *SDB* beam element has been subsequently enriched with a fibre approach and denoted as Fibre Smart Displacement Based (*FSDB*) element [29].

Given the above premises, the second aim of this paper is to further enrich the *FSDB* element to embed the discontinuous non uniform character (sequence of abrupt cross section changes) of the proposed special steel element in order to apply smart displacement shape functions to model diffusion of plasticity along *LRPD* equipped frames. The extension proposed in this work avoids any discretization of beam elements of the *LRPD* equipped frames into sub-elements as well any mesh refining during the inelastic analysis. A preliminary and preparatory study with a synthetic description of the proposed approach has been provided by the authors in [30].

The first performed application regards the check of the efficacy of the *FSDB* approach to model the *LRPD* mechanical behaviour by comparing the results obtained from *FSDB* approach with those arising from a 3D FEM analysis performed in ABAQUS environment.

In the two subsequent performed applications, the *LRPD* optimal design and the consequent analysis by *FSDB* model adopted in sizing plane steel frames with assigned elastic stiffness and limit behaviour substituting two masonry panels with different mechanical behaviors is presented. The obtained results have been checked by a comparison with those arising from a 3D FEM push-over analysis performed in ABAQUS environment. The obtained results are encouraging as regards the effectiveness of the proposed improved optimal design of the new *LRPD* as well as relatively to the modeling by means the *FSDB* approach.

2 GEOMETRICAL AND MECHANICAL CHARACTERISTICS OF THE DEVICE

All the structural elements usually adopted in steel frames possess cross sections which can be inscribed into a rectangle of dimension $b \times h$ (see, e.g., Fig. 1a where a typical I-shaped cross section is reported). Starting from this remark and taking into account that the device replaces a portion of the structural element, the overall geometry of the relevant device is assumed to be inscribed in a parallelepiped of dimensions $\ell \times b \times h$ (Fig. 1b). The connection with the structural elements is generally thought as a bolted plate and back-plate system hereinafter assumed as a perfect rigid joint, as reported in Fig. 1c, where bolts are not shown for the sake of simplicity. The core of the device, as sketched in Figs. 1b-e where the thickness

of the connection plate is indicated as ℓ_p, is constituted by a steel element whose cross-section is characterized by a piecewise geometry, with three different and subsequent I-shaped portions. The device is characterized by symmetry with respect to three orthogonal barycentric planes and it is assumed that: i) the thickness of web and flanges of the two outer portions is greater than those of the inner portion; ii) the flanges of all portions possess a unique common medium plane; iii) the webs of the three different portions have an unique common medium plane.

With reference to Fig. 1, the following geometrical characteristics are defined:

- b common base of the device portions
- h_o height of the outer portions
- h_i height of the inner portion
- ℓ_o length of the outer portions
- ℓ_i length of the inner portion
- ℓ total length of the device
- $t_{f,o}$ flange thickness of the outer portions
- $t_{f,i}$ flange thickness of the inner portion
- $t_{w,o}$ web thickness of the outer portions
- $t_{w,i}$ web thickness of the inner portion
- r_o welding radius between web and flanges of the outer portions
- r_i welding radius between web and flanges of the inner portion

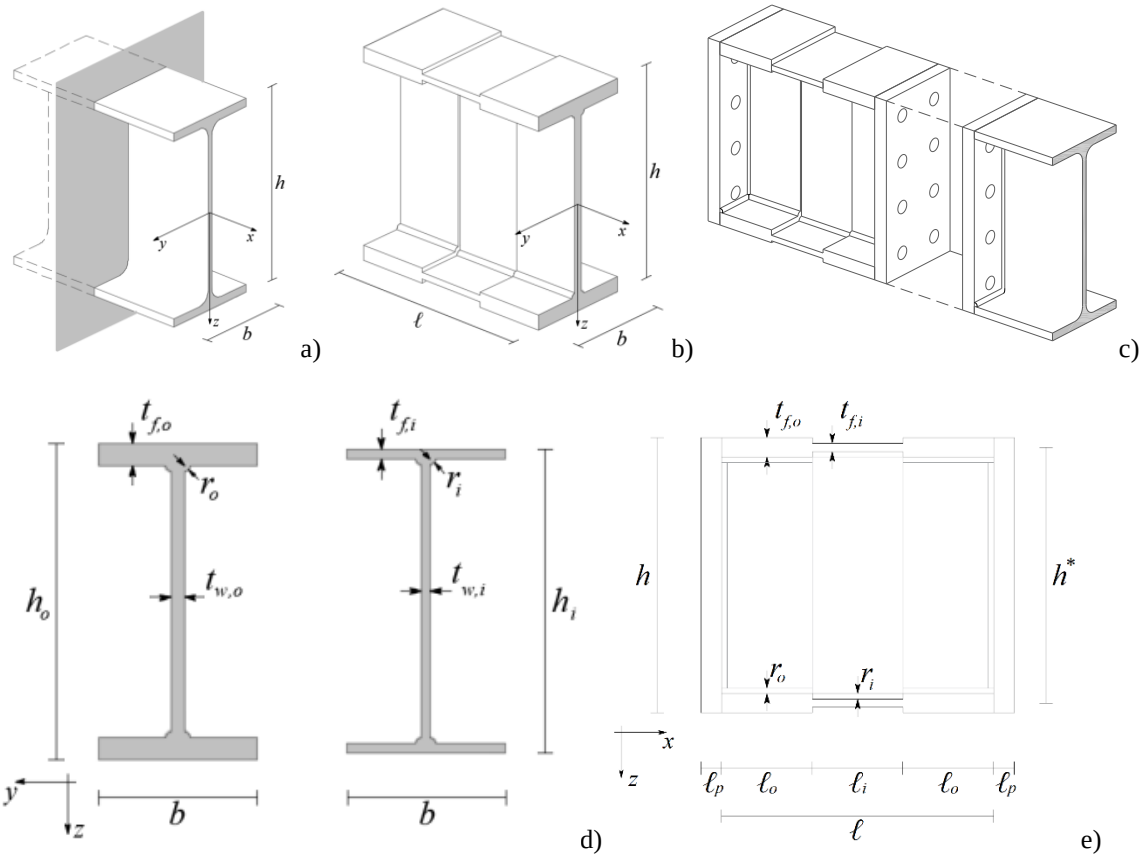


Figure 1. Sketch of the device: a) typical I-shaped steel beam element; b) 3D view; c) typical connection scheme; d) typical cross-sections; e) lateral view.

Among the geometrical characteristics of the device reported above, the welding radius has been introduced since, from a technological point of view, the device is thought, at this stage of the research, as obtained by welding of steel plates with suitable thicknesses by means, e.g., of a fully penetration welding. In the appendix all the information required to realize the *LRPD* device are reported.

For the developments of the paper, it is necessary to define the cross-section area A, the moment of inertia I, the elastic resistance modulus W_{el} and the plastic resistance modulus W_{pl}, respectively, for each portion of the device. These characteristics can be easily derived from basic geometry definitions and are not reported here for brevity's sake (see e.g. [23], [25]).

As above remarked, the proposed device must satisfy some specific requisites: i) it must exhibit an assigned limit resistance, suitably reduced with respect to that of the substituted element; ii) it must not involve any elastic flexural stiffness variation in the original substituted member; iii) it must ensure the complete plasticization of a assigned portion for the prefixed limit resistance; iv) it must be as short as possible.

The above listed requisites strongly influence the optimal geometry of the device. In what follows the geometrical and mechanical aspects related to the fulfilling of the desired device features will be discussed.

In order to characterize the mechanical behaviour of the device, for the sake of simplicity, reference is made just to plane systems, so that the device is typically subjected to axial force, shear force and bending moment. Furthermore, in this paper the influence of the shear force on the limit behaviour is neglected. Accounting for the interaction between axial and tangential stresses due to shear force, axial force and bending moment in the nonlinear plastic behaviour will be object of future developments.

For the purposes of the present paper, by assuming an elastic-perfectly plastic material behaviour, each cross section is characterized by an elastic domain and a plastic domain. Respecting the contents of the most recent international structural standards [31-32], the boundary of the elastic domain (see Fig. 2) for I-shaped cross sections in class 1, 2 and 3 is simply described by the following dimensionless conditions:

$$\left|\frac{N}{N_{el}} + \frac{M}{M_{el}}\right| = 1 \tag{1}$$

$$\left|\frac{N}{N_{el}} - \frac{M}{M_{el}}\right| = 1 \tag{2}$$

being $N_{el} = Af_y$ the elastic limit value of the axial force (coincident with the plastic limit one) and $M_{el} = W_{el}f_y$ the elastic limit value of the bending moment, with f_y the material yield stress.

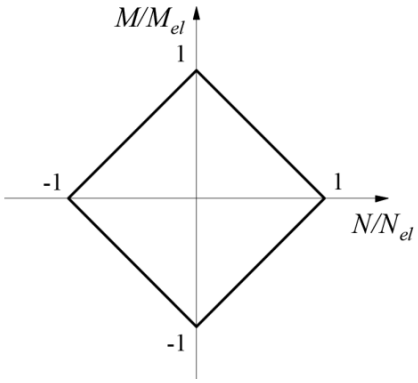


Figure 2. Dimensionless elastic domain.

For I-shaped cross sections in class 4, an analogous elastic domain can be described by the following dimensionless conditions:

$$\left|\frac{N}{N_{eff}} + \frac{M+Ne_N}{M_{eff}}\right| = 1 \tag{3}$$

$$\left|\frac{N}{N_{eff}} - \frac{M+Ne_N}{M_{eff}}\right| = 1 \tag{4}$$

being $N_{eff} = A_{eff} f_y$ and $M_{eff} = W_{eff} f_y$, with A_{eff} and W_{eff} the effective area of the cross-section subjected to uniform compression and the effective section modulus of the cross-section just subjected to bending moment, and being e_N the shift of the centroidal axis when the cross-section is subjected to compression only [33].

The boundary of the plastic domain, relative to I-shaped cross-sections in class 1 and 2, is reported in Fig. 3 and, always according with international structural standards [31-32], it is described by the following dimensionless equations:

$$\left|\frac{N}{N_{pl}} + (1-0.5a)\frac{M}{M_{pl}}\right| = 1 \tag{5}$$

$$\left|\frac{N}{N_{pl}} - (1-0.5a)\frac{M}{M_{pl}}\right| = 1 \tag{6}$$

$$\left|\frac{M}{M_{pl}}\right| = 1 \tag{7}$$

being $N_{pl} = Af_y$ the plastic limit value of the axial force, $M_{pl} = W_{pl} f_y$ the plastic limit value of the bending moment and where the parameter a is defined as follows:

$$a = \left(A - 2bt_f\right)/A \tag{8}$$

subjected to the limitation $a \leq 0.5$. It is worth noting that the size of the plateau of the domain in Fig. 3 is $2n$, and utilizing eqs. (5)-(7) it can be deduced

$$n = \frac{N}{N_{pl}} = 0.5a \tag{9}$$

and, due to the imposed constraint on parameter a, it always results $n = \frac{N}{N_{pl}} \leq 0.25$, according with the referenced standards.

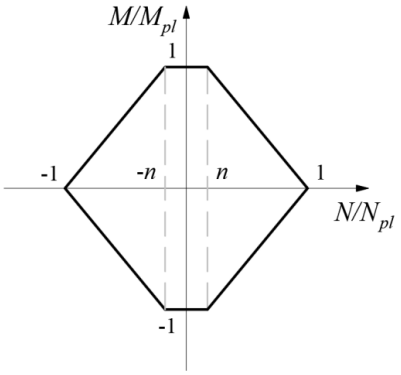


Figure 3. Dimensionless yield domain: the value of n depends on the cross-section profile ($n = 0.5a$).

Now, referring to the proposed device, analogous resistance domains can be defined and, taking into account its special geometry, just the limit behaviour of the inner portion must be checked.

Therefore, if the desired reduction of the limit resistance provided by the device is defined referring to the limit bending moment value, as usual for the flexural systems, the limit elastic behaviour can be imposed by the following relations:

$$\left|\frac{N_a}{N_{el,i}} + \frac{\alpha_{el} M_{el,p}}{M_{el,i}}\right| = 1 \tag{10}$$

$$\left|\frac{N_a}{N_{el,i}} - \frac{\alpha_{el} M_{el,p}}{M_{el,i}}\right| = 1 \tag{11}$$

being $\alpha_{el} < 1$ an appropriate assigned scalar, N_a the assigned value of the axial force, $N_{el,i}$ the elastic limit value of the axial force, $M_{el,i}$ the elastic limit value of the bending moment, both referred to the inner portion, and $M_{el,p}$ the limit elastic bending moment of the original profile. It is worth noting that the value to assign to the scalar α_{el} defines the desired reduction of the limit resistance for the device. Obviously, $N_{el,i}$ and $M_{el,i}$ must be appropriately defined basing on the relevant class of the I-shaped cross section [33]. Finally, it must be highlighted that the choice of checking the limit behaviour of the device just in terms of elastic resistance depends on the special computational finite element approach that will be utilized, as it will be clarified later on.

Moreover, in order to ensure that the device does not determine any variation in the elastic flexural stiffness of the principal beam element, it is imposed that (Fig. 4) the relative rotation $\Delta\varphi_{LRPD}$ between the bound sections of the device subjected to the bending moment $M = 1$ evaluated as follows

$$\Delta\varphi_{LRPD} = 2\int_0^{\ell_o} \frac{1}{EI_o} dx + \int_0^{\ell_i} \frac{1}{EI_i} dx \tag{12}$$

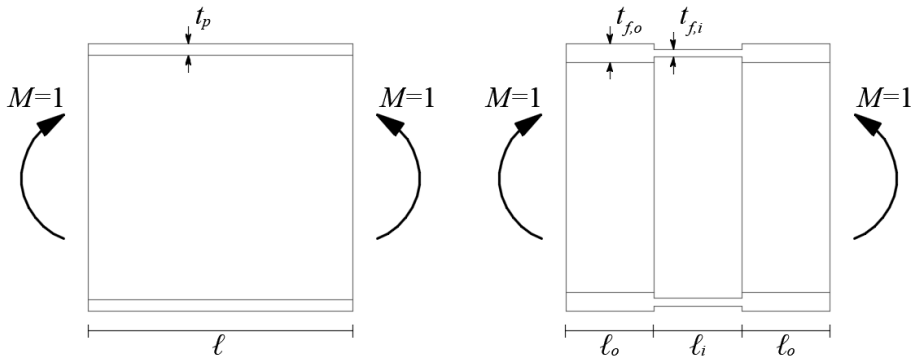
equals the one $\Delta\varphi_p$ between the end sections of the substituted original beam portion subjected to the same bending moment given as

$$\Delta\varphi_p = \int_0^{\ell} \frac{1}{EI_p} dx \tag{13}$$

where I_p is the moment of inertia of the beam section connected to the device and E is the Young's modulus of the material. As already stated in [1]-[6], the previous relations lead to the following equality:

$$\frac{\ell_i}{\ell_o} = 2\frac{I_i}{I_o}\left(\frac{I_o - I_p}{I_p - I_i}\right) \tag{14}$$

being the function on the right-hand side an increasing one with respect to I_o.



(a) (b)

Figure 4. Reference models utilized for the evaluation of the flexural stiffness: a) original profile; b) *LRPD* device.

Finally, in order to ensure the complete plasticization, at least of a section within the inner portion of the device, when the acting bending moment reaches the relevant assigned yield value, the latter should be designed with an adequate length [4]. On the other side, the further requisite that the overall length of the device must be as small as possible, such that the disturbance effect on the original structural element is minimized, must be fulfilled. Both requisites will be taken into account within the optimization problem.

3 OPTIMAL DESIGN PROBLEM FORMULATION

As widely discussed in the previous section, the *LRPD* is a device which substitutes a specific portion of the beam, and it has to satisfy the following requirements: i) it must be as short as possible, always ensuring the desired elastic plastic behaviour; ii) it must exhibit a suitably assigned resistance, lowered with respect to the one of the substituted element; iii) its global elastic flexural stiffness must be equal to that of the portion of the replaced element, being both stiffness and resistance of the device independent of each other.

Taking into account the above listed requirements, the new design problem is formulated as the search for the minimum volume of the device subjected to constraints which ensure the fulfillment of the required features appropriate to the proposed enhanced model.

The design variables involved in the optimization problem are: the height of the outer portions h_o, the height of the inner portion h_i, the length of the outer portions ℓ_o, the length of the inner portion ℓ_i, the flange thickness of the outer portions $t_{f,o}$, the flange thickness of the inner portion $t_{f,i}$, the web thickness of the outer portions $t_{w,o}$, the web thickness of the inner portion $t_{w,i}$.

Actually, the number of the design variables can be usefully reduced by utilizing the positions previously imposed on the geometrical features of the device and by following usual technological standards characterizing the I-shaped steel sections. Indeed, taking into account that the flanges of all the portions must possess a unique common medium plane, instead of the

two design variables h_o and h_i it can be suitably introduced the new design variable h^*, being h^* the distance between the medium planes of the flanges. Moreover, due to secondary influence of the web thickness on the flexural behaviour of the device, it can be imposed that, for each portion of the device, the ratio between the relevant web thickness and the flange thickness is equal to the analogous ratio characterizing the cross section of the original beam element. Finally, as usual, the welding radiuses of the different portions are imposed to be suitable fractions of the minimum thickness of the welded plates.

With the above positions, the design variable vector reduces to:

$$\boldsymbol{v}^T = \left|h^* \quad \ell_o \quad \ell_i \quad t_{f,o} \quad t_{f,i}\right| \tag{15}$$

where the symbol $(\quad)^T$ indicates the transpose of the relevant quantity, and the objective scalar function is:

$$\begin{gathered} f(\boldsymbol{v}) = 2\,A_o\ell_o + A_i\ell_i = \\ = 2\left[2bt_{f,o} + t_{w,o}\left(h_o - 2t_{f,o}\right)\right]\ell_o + \left[2bt_{f,i} + t_{w,i}\left(h_i - 2t_{f,i}\right)\right]\ell_i = \\ = 2\left[2b + \alpha_{t_p}\left(h^* - t_{f,o}\right)\right]t_{f,o}\ell_o + \left[2b + \alpha_{t_p}\left(h^* - t_{f,i}\right)\right]t_{f,i}\ell_i \end{gathered} \tag{16}$$

where b is a data of the problem and, $\alpha_{t_p} = t_{w,p}/t_{f,p}$, being $t_{f,p}$ and $t_{w,p}$ the flange and the web thicknesses of the cross section of the original beam element, respectively.

The geometrical constraints on the design variables are defined by means of the following lower bound and upper bound vectors:

$$\boldsymbol{v}_{lb}^T = |0 \quad 0 \quad \beta H \quad t_{f,p} \quad 0| \tag{17}$$

$$\boldsymbol{v}_{ub}^T = \left|\left(h - t_{f,p}\right) \quad \infty \quad \infty \quad {}^{h}/_{2} \quad {}^{h}/_{2}\right| \tag{18}$$

where, as previously stated, the lower bound on ℓ_i ensures the development of the desired plastic hinge, being $0.5 \leq \beta \leq 1$ a suitably chosen shape ratio and H the greatest transverse dimension of the beam to be substituted, while the other bounds respect the geometrical limitations prescribed in section 2.

The constraint on the limit resistance of the device can be more effectively imposed by considering a more realistic occurrence of distributed plastic deformations in the post-elastic phase, so that its mechanical limit behaviour can be designed by making reference to the elastic limit behaviour (Eqs. (10), (11)), written, as function of the design variables, as follows:

$$\left|\frac{N_a}{A_i f_y} + \frac{\alpha_{el} M_{el,p}}{W_{el,i} f_y}\right| = 1 \tag{19}$$

$$\left|\frac{N_a}{A_i f_y} - \frac{\alpha_{el} M_{el,p}}{W_{el,i} f_y}\right| = 1 \tag{20}$$

where

$$A_i = 2bt_{f,i} + \alpha_{t_p} t_{f,i}\left(h^* - t_{f,i}\right) \tag{21}$$

and

$$W_{el,i} = 2I_i/\left(h^* + t_{f,i}\right) \tag{22}$$

with

$$I_i = \frac{b\,t_{f,i}^3}{6} + \frac{b\,t_{f,i}}{2}h^{*2} + \frac{\alpha_{t_p} t_{f,i}\left(h^* - t_{f,i}\right)^3}{12} \tag{23}$$

The main novelty of the present improved optimal design formulation just regards the assignment of an appropriate value to α_{el}. Indeed, as previously reported, the necessity of ensuring the respect of the required elastic plastic behaviour for the device (i.e. the complete plasticization of a cross section within its inner portion) involves a not negligible device total length ℓ. Therefore, in order to assign the right value to α_{el}, identifying the appropriate limit bending moment values to be utilized in the optimization problems, it is necessary to account for the actual bending moment distribution which characterizes the response of the relevant frame.

Therefore, always accounting for the expected length of the device, the elastic limit bending moment to assign to the inner portion of the device $\alpha_{el}M_{el,p}$ is found by imposing the equivalence between the elastic energy produced in the inner portion of the device in the hypothesis of constant bending moment and the elastic energy produced in the same portion of the original beam element in correspondence of the chosen limit elastic behaviour, i.e. (see Fig. 5):

$$\frac{(\alpha_{el}M_{el,p})^2 \ell_i}{I_i} = \int_{\ell_o}^{\ell_o+\ell_i} \frac{[M(0)-Tx+N_a e_N]^2}{I_p}\, dx \tag{24}$$

with $e_N = 0$ for cross section class 1, 2 and 3, from which the form of α_{el} as function of the design variables can be deduced

$$\alpha_{el} = \frac{1}{M_{el,p}} \left(\frac{I_i}{\ell_i I_p} \int_{\ell_o}^{\ell_o+\ell_i} [M(0) - Tx + N_a e_N]^2\, dx \right)^{\frac{1}{2}} \tag{25}$$

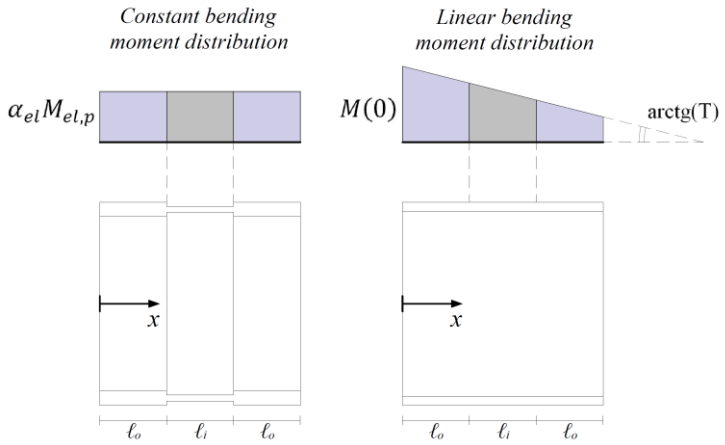


Fig. 5. Adopted model for the imposed elastic energy equivalence.

Based on the above reported positions, the optimal design problem for *LRPD* can be formulated as follows: assigned the cross section of the beam element to be substituted, given β, α_{t_p}, N_a, find

$$\min_{(\boldsymbol{v})} f(\boldsymbol{v}) \tag{26}$$

subjected to:

$$\boldsymbol{v}_{lb} \leq \boldsymbol{v} \leq \boldsymbol{v}_{ub} \tag{27}$$

$$\boldsymbol{A}_{in}\boldsymbol{v} \leq \boldsymbol{c}_{in} \tag{28}$$

$$G_{eq}(\boldsymbol{v}) = 1 \tag{29}$$

$$G_{in}(\boldsymbol{v}) \leq 0 \tag{30}$$

Eq. (27) defines appropriate geometrical constraints on the design variables by means of the already defined lower and upper bound vectors.

Eq. (28) represents the linear inequality constraints which guarantee that $t_{f,o} \geq t_{f,i}$, and that the maximum height of the cross section device is not greater than the height of the cross section of the substituted beam element, where the matrix $\boldsymbol{A}_{in}$ has the form:

$$\boldsymbol{A}_{in} = \begin{vmatrix} 0 & 0 & 0 & -1 & 1 \\ 1 & 0 & 0 & 1 & 0 \end{vmatrix} \tag{31}$$

and the vector of the known terms is:

$$\boldsymbol{c}_{in} = \begin{vmatrix} 0 \\ h \end{vmatrix} \tag{32}$$

Eq. (29) is nonlinear equality constraint through which the chosen elastic limit bending moment is imposed for the device, given by

$$G_{eq}(\boldsymbol{v}) = \gamma_N \frac{N_a}{A_i(\boldsymbol{v}) f_y} + \gamma_M \frac{\left\{\frac{I_i(\boldsymbol{v})}{\ell_i I_p} \int_{\ell_o}^{\ell_o+\ell_i} [M(0) - Tx + N_a e_N]^2 dx\right\}^{\frac{1}{2}}}{W_{el,i}(\boldsymbol{v}) f_y} \tag{33}$$

being γ_N and γ_M two scalars whose values are 1 or -1 depending on which quadrant of the elastic domain is interested by the given N_a and the calculated bending moment.

Finally, Eq. (30) describes the nonlinear inequality constraint related to the equivalence of the elastic bending stiffness of the device and the analogous quantity of the substituted beam element, being

$$G_{in}(\boldsymbol{v}) = \frac{\ell_i}{\ell_o} - 2\frac{I_i(\boldsymbol{v})}{I_o(\boldsymbol{v})}\left(\frac{I_o(\boldsymbol{v}) - I_p}{I_p - I_i(\boldsymbol{v})}\right) \tag{34}$$

the nonlinear constraint function.

In the application stage, the proposed formulation will be applied for the determination of the *LRPD* optimal design to be utilized for the sizing of a plane steel frame with assigned elastic stiffness and limit behaviour.

4 THE SMART DISPLACEMENT BASED (*SDB*) BEAM ELEMENT TO MODEL BEAMS WITH *LRPD* DEVICES

The *LRPD* device, presented and discussed in the previous sections, has been optimised with appropriate abrupt variations of cross sections and specifically designed to undergo plastic deformations mainly in the inner core. In order to perform numerical analysis of a frame equipped with *LRPD* devices, each frame element should be modeled as a discontinuous beam characterised by piecewise constant cross sections. The latter discontinuities occur between the outer and the inner portions of the *LRPD* devices however additional discontinuities, during the nonlinear analysis, are encountered at those cross sections suffering stiffness decay due to the onset of plastic deformations. Along axis discontinuity of beams are usually dealt with by formulating the governing differential equations over portions of the beam and enforcing the

relevant continuity conditions between adjacent segments. Alternatively, Finite Element Model (FEM) is widely adopted and more efficacious when discontinuous frames, rather than simple beams, are analysed. Within the context of standard displacement based FEM, the displacement field of each beam finite element is described by Hermite polynomial shape functions leading to the definition of the element stiffness matrix [18]- [22]. Although the element stiffness matrix is updated during the step-by step nonlinear analysis (tangent stiffness matrix) relying on integration of the constitutive laws at pre-established Gauss integration cross sections, the displacement shape functions are invariant with the analysis without accounting for the along axis stiffness variations of the beam element. Improvement of the performance of the FEM both for uniform beams and, more significantly, for non-uniform discontinuous beams can be obtained by means of a preliminary mesh refinement or, alternatively, an a-posteriori sub-discretisation during the nonlinear analysis as well as an appropriate Gauss point refinement [34]-[39]. To overcome the latter problems some of the authors recently formulated a Smart Displacement Based (*SDB*) beam element, with uniform cross section, endowed with adaptive displacement shape functions able to update during the inelastic analysis [28]-[29]. The proposed adaptive displacement shape functions coincide, in the initial linear elastic state, with the classical Hermite polynomials and evolve subsequently in accordance with the stiffness decay evaluated at the Gauss cross sections. The advantage of such beam element consists in avoiding any FE remeshing or Gauss point refinement during the analysis. In the case of frames equipped with *LRPD* devices, the additional complicacy related to the discontinuous character of the beam elements has to be accounted for. With this aim, the *SDB* element is further enriched in this work to embed the non-uniform character of the beam element by formulating displacement shape function accounting for the along axis cross section discontinuities.

Although the classical Timoshenko theory to account for the shear deformations of discontinuous beam elements has been considered by the authors to conduct linear elastic analyses [40]-[41], in this context the Euler-Bernoulli beam model is considered to account for discontinuities in the nonlinear analysis. Further complicacy due to the shear-flexural coupling in the nonlinear behavior, as treated in the literature in [42]-[44] in absence of discontinuities, requires the present study before its introduction for the nonlinear analysis of *LRPD* devices.

4.1 A model for discontinuous Euler-Bernoulli beams with *LRPD* devices

The Euler-Bernoulli beam model, with along axis variable axial $EA(x)$ and flexural $EI(x)$ stiffness, capable of capturing the effect of stepped cross sections by means of the use of generalised functions (distributions), is adopted in this work [45]. E, A, I represent the Young modulus, the area and the moment of inertia of the cross section at abscissa x spanning from 0 to the length L of the beam, respectively. The beam model adopted in this work to describe a beam endowed with two *LRPD* devices at the two ends is characterised by 7 segments (Fig. 6) with different axial and flexural stiffness denoted as EA_j, EI_j for $x_j < x < x_{j+1}\ j = 1, \dots, 7$, respectively, at the following cross sections

$$
\begin{aligned}
x_1 &= 0 \\
x_2 &= \ell_o \\
x_3 &= \ell_o + \ell_i \\
x_4 &= 2\ell_o + \ell_i \\
x_5 &= 2\ell_o + \ell_i + \ell_b \\
x_6 &= 3\ell_o + \ell_i + \ell_b \\
x_7 &= 3\ell_o + 2\ell_i + \ell_b \\
x_8 &= \ell
\end{aligned}
\tag{35}
$$

The above beam model is usually denoted as stepped beam model, since characterized by geometric changes of the cross section, and the relevant axial and flexural stiffness can be formulated by making use of the well know Heaviside (unit step) generalised function $U(x - x_j)$, (defined as $U(x - x_j) = 0$ for $x < x_j$; $U(x - x_j) = 1$ for $x > x_j$) as follows:

$$EA(x) = EA_o\left[1 - \sum_{j=1}^{7}(\alpha_{x,j} - \alpha_{x,j-1})U(x - x_j)\right] \tag{36}$$

$$EI(x) = EI_o\left[1 - \sum_{j=1}^{7}(\alpha_{z,j} - \alpha_{z,j-1})U(x - x_j)\right] \tag{37}$$

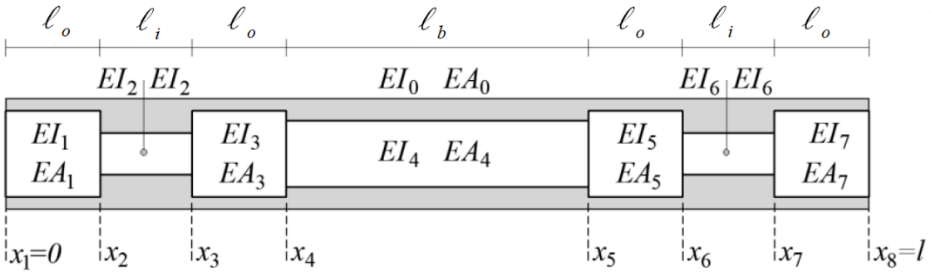


Figure 6: Stepped axial-flexural beam.

In Eqs. (36),(37), $\alpha_{x,j} = \frac{EA_o - EA_j}{EA_o}$, $\alpha_{z,j} = \frac{EI_o - EI_j}{EI_o}$, $j = 1, \dots, 7$ with $0 \le \alpha_{x,j} \le 1$, with represent the normalized variation of the current axial and flexural stiffness with respect to the reference values EA_o and EI_o, respectively. The difference $\alpha_{x,j} - \alpha_{x,j-1}$ $\alpha_{z,j} - \alpha_{z,j-1}$ denote the relevant axial and bending stiffness abrupt variations at cross sections x_j $j = 1, \dots, 7$.

However, each of the segments of the stepped beam may undergo axial and flexural stiffness degradation due to occurrence of plastic deformations. Exact integration of nonlinear elastic, perfectly plastic beams has been provided in a very limited number of cases restricted to uniform beams [46]. The latter problem is usually solved in approximate way in accordance to a step-by step integration of the nonlinear elastic-plastic constitutive equations at preselected Gauss cross sections whose number and positions depends on the desired accuracy. For the case at hand, a Gauss integration scheme for the integration of the nonlinear constitutive laws of the type Gauss-Legendre for those segments which are expected to behave elastically, while the Gauss-Lobatto scheme for the inner core of the device which specifically designed to undergo plastic deformations. The distribution of $n_G = 16$ Gauss cross sections at abscissae $x_{G,i}, i = 1, \dots, n_G$ assumed for the stepped beam in Fig. 6 is depicted in Fig. 7. Depending on the choice of the Gauss cross sections, the stepped beam will be subdivided into $n_G = 16$ sub-segments whose length is defined by the relevant Gauss weight length $l_{G,i}, i = 1, \dots, n_G$. Each sub-segment is prone to uniform axial and flexural stiffness degradation in accordance to the

integration of the constitutive law at the pertinent Gauss cross section.

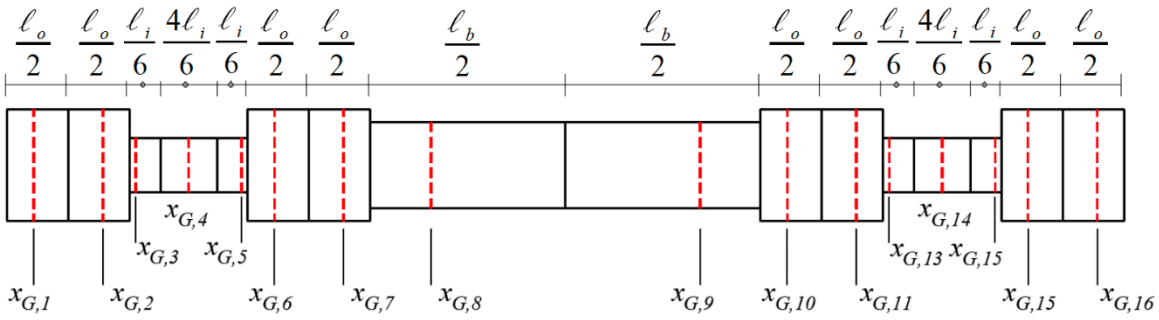


Figure 7: Beam element with *LRPD* devices and Gauss integration cross sections.

In order to account for the stiffness degradation due to the occurrence of plastic deformations, the stepped beam model with the cross section discontinuities due to the *LRPD* devices formulated in Eqs. (36),(37) can be further enriched by means of the introduction of additional degradation parameters $\beta_{x,i}, \beta_{z,i}, i = 1, \dots, n_G$ into the axial and flexural stiffness as follows:

$$EA(x) = EA_o\left[1 - \sum_{j=1}^{7}(\alpha_{x,j} - \alpha_{x,j-1})U(x - x_j) - \sum_{i=1}^{n_G}(\beta_{x,i} - \beta_{x,i-1})U(x - x_{d,i})\right] \quad (38)$$

$$EI(x) = EI_o\left[1 - \sum_{j=1}^{7}(\alpha_{z,j} - \alpha_{z,j-1})U(x - x_j) - \sum_{i=1}^{n_G}(\beta_{z,i} - \beta_{z,i-1})U(x - x_{d,i})\right] \quad (39)$$

where the abscissae denoted as $x_{d,i}, i = 1, \dots, n_G$ indicate the cross sections where the axial and flexural stiffness degradation discontinuities may occur in accordance to the scheme in Fig.6 and defined as follows:

$$\begin{aligned}
x_{d,1} &= 0 & x_{d,9} &= 2\ell_o + \ell_i + \ell_b/2 \\
x_{d,2} &= \ell_o/2 & x_{d,10} &= [2\ell_o + \ell_i + \ell_b]^+ \\
x_{d,3} &= \ell_o^+ & x_{d,11} &= 5\ell_o/2 + \ell_i + \ell_b \\
x_{d,4} &= \ell_o + \ell_i/6 & x_{d,12} &= [3\ell_o + \ell_i + \ell_b]^+ \\
x_{d,5} &= \ell_o + 5\,\ell_i/6 & x_{d,13} &= 3\ell_o + 7\,\ell_i/6 + \ell_b \\
x_{d,6} &= [\ell_o + \ell_i]^+ & x_{d,14} &= 3\ell_o + 11\,\ell_i/6 + \ell_b \\
x_{d,7} &= 3\ell_o/2 + \ell_i & x_{d,15} &= [3\ell_o + 2\ell_i + \ell_b]^+ \\
x_{d,8} &= [2\ell_o + \ell_i]^+ & x_{d,16} &= 7\ell_o/2 + 2\ell_i + \ell_b
\end{aligned} \quad (40)$$

where, in order to evaluate the Heaviside functions appearing in Eqs. (51),(52), the apex "+" indicates the abscissa immediately at the right of the cross section in parenthesis. The $\beta_{x,i}, \beta_{z,i}$ parameters introduced in Eqs. (38),(39) take the initial values $\beta_{x,i} = 0, \beta_{z,i} = 0$ corresponding to a fully elastic state and are subjected to a step-by-step updating within the range $0 \leq \beta_{x,i} \leq 1{,}0 \leq \beta_{z,i} \leq 1$, as described in the following subsections, being $\beta_{x,i} = 1, \beta_{z,i} = 1$ correspondent to a fully plastic state of the relevant Gauss cross section.

The first step of the formulation of the new nonlinear beam element to model beams with *LRPD* devices requires the expression of the closed form solution of the linear elastic response. To this purpose the adoption of the stepped beam model with additional sub-segments as in Eqs. (38),(39) allows the formulation of the static governing equations in presence of axial $p_x(x)$ and transversal $p_z(x)$ load distributions as follows:

$$EA_o\left\{\left[1-\sum_{j=1}^{7}\left(\alpha_{x,j}-\alpha_{x,j-1}\right)U\left(x-x_j\right)-\sum_{i=1}^{n_G}\left(\beta_{x,i}-\beta_{x,i-1}\right)U\left(x-x_{d,i}\right)\right]u_x^I(x)\right\}^I = -p_x(x) \quad (41)$$

$$EI_o\left\{\left[1-\sum_{j=1}^{7}\left(\alpha_{z,j}-\alpha_{z,j-1}\right)U\left(x-x_j\right)-\sum_{i=1}^{n_G}\left(\beta_{z,i}-\beta_{z,i-1}\right)U\left(x-x_{d,i}\right)\right]u_z^{II}(x)\right\}^{II} = p_z(x) \quad (42)$$

where the apex indicates the differentiation with respect to x and $u_x\ (x)$, $u_z\ (x)$ are the axial displacement and the transversal deflection functions.

Eqs. (41),(42) can be integrated as follows:

$$u_x^I(x) = -\frac{1}{E_oA_o}\frac{\left[p_x^{[1]}(x)+d_1\right]}{\left[1-\sum_{j=1}^{7}\left(\alpha_{x,j}-\alpha_{x,j-1}\right)U\left(x-x_j\right)-\sum_{i=1}^{n_G}\left(\beta_{x,i}-\beta_{x,i-1}\right)U\left(x-x_{d,i}\right)\right]} \quad (43)$$

$$u_z^{II}(x) = -\frac{1}{E_oI_o}\frac{\left[p_z^{[2]}(x)+b_1x+b_2\right]}{\left[1-\sum_{j=1}^{7}\left(\alpha_{z,j}-\alpha_{z,j-1}\right)U\left(x-x_j\right)-\sum_{i=1}^{n_G}\left(\beta_{z,i}-\beta_{z,i-1}\right)U\left(x-x_{d,i}\right)\right]} \quad (44)$$

where d_1, b_1, b_2 are integration constants and $p_x^{[k]}(x), p_z^{[k]}(x)$ indicate the k-th primitive functions of the relevant external load distributions $p_x(x), p_z(x)$, respectively.

Eqs. (43),(44), according to the generalised function integration rules [47]-[48], lead to the following expressions:

$$u_x^I(x) = -\left[1+\sum_{j=1}^{7}\left(\frac{\alpha_{x,j}}{1-\alpha_{x,j}}-\frac{\alpha_{x,j-1}}{1-\alpha_{x,j-1}}\right)U\left(x-x_j\right)+\sum_{i=1}^{n_G}\left(\frac{\beta_{x,i}}{1-\beta_{x,i}}-\frac{\beta_{x,i-1}}{1-\beta_{x,i-1}}\right)U\left(x-x_{d,i}\right)\right]\left[\frac{p_x^{[1]}(x)}{E_oA_o}+\frac{d_1}{E_oA_o}\right] \quad (45)$$

$$u_z^{II}(x) = \left[1+\sum_{j=1}^{7}\left(\frac{\alpha_{z,j}}{1-\alpha_{z,j}}-\frac{\alpha_{z,j-1}}{1-\alpha_{z,j-1}}\right)U\left(x-x_j\right)+\sum_{i=1}^{n_G}\left(\frac{\beta_{z,i}}{1-\beta_{z,i}}-\frac{\beta_{z,i-1}}{1-\beta_{z,i-1}}\right)U\left(x-x_{d,i}\right)\right]\left[\frac{p_z^{[2]}(x)}{E_oI_o}+\frac{b_1x}{E_oI_o}+\frac{b_2}{E_oI_o}\right] \quad (46)$$

Integration of Eqs. (45),(46), in view of the integration rules of the distributions and after simple algebra, leads to the following explicit expressions for the axial displacement and the transversal deflection functions $u_x(x), u_z(x)$, respectively:

$$u_x(x) = a_1 + a_2g_2\left(x;\beta_{x,j}\right) + g_3\left(x;\beta_{x,j}\right) \quad (47)$$

$$u_z\ (x) = c_1 + c_2x + c_3f_3\left(x;\beta_{z,j}\right) + c_4f_4\left(x;\beta_{z,j}\right) + f_5\left(x;\beta_{z,j}\right) \quad (48)$$

where the additional constants a_1, c_1, c_2 have been introduced while other integration constants have been re-defined as follows: $a_2 = d_1/(E_oA_o)$, $c_3 = b_2/(2E_oI_o)$, $c_4 = b_1/(6E_oI_o)$.

In Eqs. (47),(48) the functions $g_2\left(x;\beta_{x,i}\right), g_3\left(x;\beta_{x,i}\right), f_3\left(x;\beta_{z,i}\right), f_4\left(x;\beta_{z,i}\right), f_5\left(d_1\beta_{z,i}\right)$ are defined as follows:

$$g_2\left(x;\beta_{x,i}\right) = -x - \sum_{j=1}^{7}\left(\frac{\alpha_{x,j}}{1-\alpha_{x,j}}-\frac{\alpha_{x,j-1}}{1-\alpha_{x,j-1}}\right)\left(x-x_j\right)U\left(x-x_j\right) + \sum_{i=1}^{n_G}\left(\frac{\beta_{x,i}}{1-\beta_{x,i}}-\frac{\beta_{x,i-1}}{1-\beta_{x,i-1}}\right)\left(x-x_{d,i}\right)U\left(x-x_{d,i}\right) \quad (49)$$

$$g_3\left(x;\beta_{x,i}\right) = -\frac{p_x^{[2]}(x)}{E_oA_o} - \sum_{j=1}^{7}\frac{1}{E_oA_o}\left(\frac{\alpha_{x,j}}{1-\alpha_{x,j}}-\frac{\alpha_{x,j-1}}{1-\alpha_{x,j-1}}\right)\left(p_x^{[2]}(x)-p_x^{[2]}\left(x_j\right)\right)U\left(x-x_j\right) - \sum_{i=1}^{n_G}\frac{1}{E_oA_o}\left(\frac{\beta_{x,i}}{1-\beta_{x,i}}-\frac{\beta_{x,i-1}}{1-\beta_{x,i-1}}\right)\left(p_x^{[2]}(x)-p_x^{[2]}\left(x_{d,i}\right)\right)U\left(x-x_{d,i}\right) \quad (50)$$

$$f_3(x;\beta_{z,i}) = x^2 + \sum_{j=1}^{7}\left(\frac{\alpha_{z,j}}{1-\alpha_{z,j}} - \frac{\alpha_{z,j-1}}{1-\alpha_{z,j-1}}\right)(x-x_j)^2 U(x-x_j) + \sum_{i=1}^{n_G}\left(\frac{\beta_{z,i}}{1-\beta_{z,i}} - \frac{\beta_{z,i-1}}{1-\beta_{z,i-1}}\right)(x-x_{d,i})^2 U(x-x_{d,i}) \quad (51)$$

$$f_4(x;\beta_{z,i}) = x^3 + \sum_{j=1}^{7}\left(\frac{\alpha_{z,j}}{1-\alpha_{z,j}} - \frac{\alpha_{z,j-1}}{1-\alpha_{z,j-1}}\right)(x^3 - 3x_j^2 x + 2x_j^3)U(x-x_j) + \sum_{i=1}^{n_G}\left(\frac{\beta_{z,i}}{1-\beta_{z,i}} - \frac{\beta_{z,i-1}}{1-\beta_{z,i-1}}\right)(x^3 - 3x_{d,i}^2 x + 2x_{d,i}^3)U(x-x_{d,i}) \quad (52)$$

$$f_5(x;\beta_{z,i}) = \frac{p_z^{[4]}(x)}{E_o I_o} + \sum_{j=1}^{7}\frac{1}{E_o I_o}\left(\frac{\alpha_{z,j}}{1-\alpha_{z,j}} - \frac{\alpha_{z,j-1}}{1-\alpha_{z,j-1}}\right)\left[p_z^{[4]}(x) - p_z^{[4]}(x_j)\right]U(x-x_j) + \sum_{i=1}^{n_G}\frac{1}{E_o I_o}\left(\frac{\beta_{z,i}}{1-\beta_{z,i}} - \frac{\beta_{z,i-1}}{1-\beta_{z,i-1}}\right)\left[p_z^{[4]}(x) - p_z^{[4]}(x_{d,i})\right]U(x-x_{d,i}) - \sum_{j=1}^{7}\left(\frac{\alpha_{z,j}}{1-\alpha_{z,j}} - \frac{\alpha_{z,j-1}}{1-\alpha_{z,j-1}}\right)p_z^{[3]}(x)(x-x_j)U(x-x_j) - \sum_{i=1}^{n_G}\left(\frac{\beta_{z,i}}{1-\beta_{z,i}} - \frac{\beta_{z,i-1}}{1-\beta_{z,i-1}}\right)p_z^{[3]}(x)(x-x_{d,i})U(x-x_{d,i}) \quad (53)$$

where the dependence on the parameters $\beta_{x,i}$ and $\beta_{z,i}$ have been evidenced in view of the updating required by the nonlinear analysis originated by onset of plastic deformations at Gauss integration points.

Eqs. (47),(48) represent the explicit elastic solution of the stepped beam, with two *LRPD* devices, in terms of axial and transversal displacements that do not require enforcement of any continuity condition as well as any along axis discretisation. The role of the parameters $\beta_{x,i}$ and $\beta_{z,i}$ consists in an interactive modification of the elastic response ruled by integration of the nonlinear constitutive laws at Gauss cross sections. The latter explicit solution can hence be easily adopted for the definition of a nonlinear finite beam element embedding the stiffness variations due the diffusion of plastic deformations along the beam axis.

4.2 The Smart Displacement Shape Functions (*SDSF*s)

The stepped beam model introduced in the last sub-section is here adopted to define a beam element, connecting joints i and j, and defined in the x,z plane as shown in Fig. 8. The nodal displacements q_k, $k = 1,\dots,6$ as in Fig. 4a, and the nodal forces Q_k, $k = 1,\dots,6$, as in Fig. 8b, are collected in the vectors $\mathbf{q}_e$, $\mathbf{Q}_e$ respectively.

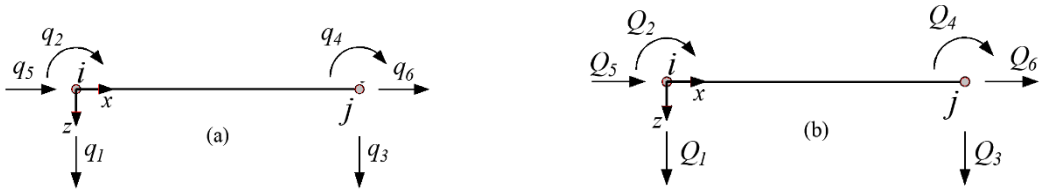


Figure 8: Nodal degrees of freedom (a) and dual forces (b) of the element.

The displacement field of the beam element proposed to model the beam with *LRPD* devices is obtained by formulating the so-called displacement shape functions $N_k(x)$, $k = 1,\dots,6$. The latter are defined in turn as the contributions to the axial and transversal displacement functions of unit nodal displacements. Given that, on account of the closed form solution provided in Eqs. (47)-(53), the axial $u_x(x)$ and transversal $u_z(x)$ displacement functions can be expressed as follows:

$$u_x(x) = N_5(x;\beta_{x,i})q_5 + N_6(x;\beta_{x,i})q_6 \tag{54}$$

$$u_z(x) = N_1(x;\beta_{z,i})q_1 + N_2(x;\beta_{z,i})q_2 + N_3(x;\beta_{z,i})q_3 + N_4(x;\beta_{z,i})q_4 \tag{55}$$

where the shape functions $N_k(x), k = 1,\dots,6$ have been derived by the solution in Eqs. (47),(48), in absence of external load, by imposing unit boundary displacements to evaluate the integration constants and are given by:

$$N_1(x;\beta_{z,i}) = 1 - \frac{f_4'(L;\beta_{z,i})}{\kappa} f_3(x;\beta_{z,i}) + \frac{f_3'(L;\beta_{z,i})}{\kappa} f_4(x;\beta_{z,i}) \tag{56}$$

$$N_2(x;\beta_{z,i}) = x + \frac{-Lf_4'(L;\beta_{z,i}) + f_4\ (L;\beta_{z,i})}{\kappa} f_3(x;\beta_{z,i}) + \frac{-f_3\ (L;\beta_{z,i}) + Lf_3'(L;\beta_{z,i})}{\kappa} f_4(x;\beta_{z,i}) \tag{57}$$

$$N_3(x;\beta_{z,i}) = \frac{f_4'(L;\beta_{z,i})}{\kappa} f_3(x;\beta_{z,i}) - \frac{f_3'(L;\beta_{z,i})}{\kappa} f_4(x;\beta_{z,i}) \tag{58}$$

$$N_4(x;\beta_{z,i}) = -\frac{f_4\ (L;\beta_{z,i})}{\kappa} f_3(x;\beta_{z,i}) + \frac{f_3\ (L;\beta_{z,i})}{\kappa} f_4(x;\beta_{z,i}) \tag{59}$$

$$N_5(x;\beta_{x,i}) = 1 - \frac{1}{g_2(L;\beta_{x,i})} g_2(x;\beta_{x,i}) \tag{60}$$

$$N_6(x;\beta_{x,i}) = \frac{1}{g_2(L;\beta_{x,i})} g_2(x;\beta_{x,i}) \tag{61}$$

where the following position has been made:

$$\kappa = f_3\ (L;\beta_{z,i}) f_4'(L;\beta_{z,i}) - f_4\ (L;\beta_{z,i}) f_3'(L;\beta_{z,i}) \tag{62}$$

Eqs. (54)-(62) show the dependency of the displacement shape functions on the stiffness decay parameters $\beta_{x,i}$ and $\beta_{z,i}$ in view of the definition of the functions $g_2(x;\beta_{x,i})$, $g_3(x;\beta_{x,i}), f_3(x;\beta_{z,i}), f_4(x;\beta_{z,i}), f_5(x;\beta_{z,i})$ provided by Eqs. (49)-(53).

It has to be noted that the proposed shape functions, in accordance to what required by discontinuous cross sections due to the presence of *LRPD* devices, both for transversal and axial displacements, are characterized by discontinuous derivatives in view of the definition of the distributional terms appearing in the functions $g_2(x;\beta_{x,i})$, $f_3(x;\beta_{z,i}), f_4(x;\beta_{z,i})$ defined in Eqs. (49), (51), (52), respectively. The above, transversal and axial, shape functions are hence not regular smooth functions at the beginning of the analysis (due to the parameters $\alpha_{z,j}$, α_{xj}) and, furthermore, are prone to evolve, in accordance to the parameters $\beta_{z,i}$, $\beta_{x,i}$, towards further irregularities at the onset of plastic deformations.

Based on the formulation of the displacement shape functions in Eqs. (69)-(74), the vector of generalised deformation components $\mathbf{d}(x) = [\varepsilon_0(x) \quad \chi_y(x)]^T$, collecting the discontinuous axial deformation $\varepsilon_0(x)$ of the beam geometrical axis and the discontinuous curvature $\chi_y(x)$ of the proposed plane beam element, can be expressed in terms of nodal displacements, by accounting for the standard Euler-Bernoulli model relationships, as follows:

$$\mathbf{d}(x) = \mathbf{B}(x;\beta_{x,i},\beta_{z,i})\,\mathbf{q}_e \tag{63}$$

where the matrix $\mathbf{B}(x;\beta_{x,i},\beta_{z,i})$, also dependent on the stiffness decay parameters $\beta_{x,i}$ and $\beta_{z,i}$ is defined in terms of derivatives of the displacement shape functions as follows:

$$\mathbf{B}(x;\boldsymbol{\beta}) = \begin{bmatrix} 0 & 0 & 0 & 0 & N_5'(x;\beta_{x,i})N_6'(x;\beta_{x,i}) \\ -N_1''(x;\beta_{z,i}) & -N_2''(x;\beta_{z,i}) & -N_3''(x;\beta_{z,i}) & -N_4''(x;\beta_{z,i}) & 0 \quad 0 \end{bmatrix} \tag{64}$$

A crucial step in the formulation of the proposed element consists in the evaluation of the

stiffness variation and the consequent updating of the parameters $\beta_{x,i}$, $\beta_{z,i}$ at each step based on a nonlinear state determination at the chosen Gauss cross sections. The displacement shape function defined in Eqs. (56)-(61) are hence subject to updating together with the parameters $\beta_{x,i}$, $\beta_{z,i}$, and, for this reason, they are addressed to as Smart Displacement Shape Functions (*SDSF*s).

4.3 The element stiffness matrix by means of a fibre approach

According to a fibre approach, each Gauss cross section is discretised into n_f strips (denoted as fibres), as in Fig. 9, characterised by an area A_f, $f = 1, \dots, n_f$ and a nonlinear uniaxial stress-strain constitutive behaviour.

By assuming the principle of planar section conservation, and in view of Eq. (62), providing the generalised deformation component expressed in terms of nodal displacements $\mathbf{q_e}$, the axial strain $\varepsilon_x(x)$ of each fibre is written as:

$$\varepsilon_x(x; z_f) = \boldsymbol{\alpha}(z_f)\, \mathbf{B}(x; \beta_x, \beta_z)\, \mathbf{q}_e \tag{65}$$

where the row vector $\boldsymbol{\alpha}(z_f) = [1 \quad z_f]$, dependent on the distance z_f of the *f*-th fibre from the beam axis, has been introduced.

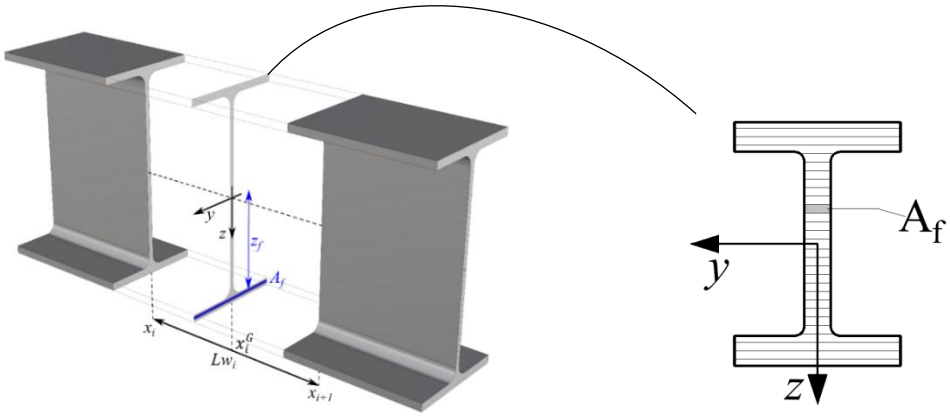


Figure 9: Fibre discretization of cross section according to a 2D formulation.

By standard application of the principle of virtual displacements, and in view of the adopted Gauss integration scheme, the element stiffness matrix $\mathbf{K}_e(\beta_{x,i}, \beta_{z,i})$ is obtained as follows:

$$\mathbf{K}_e(\beta_{x,i}, \beta_{z,i}) \approx L \sum_{i=1}^{n_G} \mathbf{B}^{\boldsymbol{T}}(x_{G,i}; \beta_{x,i}, \beta_{z,i}) \mathbf{k}(x_{G,i}) \mathbf{B}(x_{G,i}; \beta_{x,i}, \beta_{z,i}) w_r \tag{66}$$

As result of the adopted *SDSF*s, the element stiffness matrix $\mathbf{K}_e(\beta_{x,i}, \beta_{z,i})$, differently from the classical displacement-based approach commonly adopted in the literature, depends on the variation of the shape functions which are updated according to the parameters $\beta_{x,i}, \beta_{z,i}$. The inner matrix $\mathbf{k}(x_{G,i})$ appearing in Eq. (66), evaluated at the Gauss cross sections, represents the cross-section stiffness matrix and is given, due to the adopted fibre discretisation, as follows:

$$\begin{aligned} \mathbf{k}(x_{G,i}) &= \sum_{f=1}^{n_f} \boldsymbol{\alpha}^{\boldsymbol{T}}(z_f) E_T(x_{G,i}, z_f) A_f \boldsymbol{\alpha}(z_f) \\ &= \begin{bmatrix} \sum_{f=1}^{n_f} E_T(x_{G,i}, z_f) A_f & \sum_{f=1}^{n_f} E_T(x_{G,i}, z_f) A_f z_f \\ \sum_{f=1}^{n_f} E_T(x_{G,i}, z_f) A_f z_f & \sum_{f=1}^{n_f} E_T(x_{G,i}, z_f) A_f z_f^2 \end{bmatrix} \end{aligned} \tag{67}$$

where E_T indicates the tangent modulus of the nonlinear axial stress-axial strain relationship modelling the constitutive behaviour of each cross-section fibre.

The cross section stiffness matrix $\mathbf{k}(x_{G,i})$ at each Gauss cross section is evaluated by performing a parallel integration of the uniaxial nonlinear constitutive laws at each fibre in the step-by-step analysis that delivers the current tangent stiffness modulus $E_T(x; z_f)$ appearing in Eq. (67). Finally, once integration of the nonlinear constitutive laws has been performed at fibre level, the updating of the stiffness parameters $\beta_{x,i}$, $\beta_{z,i}$, is obtained straightforwardly, by accounting for the coupling between the axial and flexural behaviour, as follows:

$$\beta_{x,j} = 1 - \frac{1}{E_0 A_0}\left[\sum_{f=1}^{n_f} E_T(x_{G,i}; z_f) A_f + \sum_{f=1}^{n_f} E_T(x_{G,i}; z_f) A_f \, z_f \frac{\mathrm{d}\chi_y}{\mathrm{d}\varepsilon_0}\right] \tag{68}$$

$$\beta_{z,i} = 1 - \frac{1}{E_0 I_0}\left[\sum_{f=1}^{n_f} E_T(x_{G,i}; z_f) A_f \, z_f \frac{\mathrm{d}\varepsilon_0}{\mathrm{d}\chi_y} + \sum_{f=1}^{n_f} E_T(x_{G,i}; z_f) A_f \, z_f^2\right] \tag{69}$$

in terms of the current tangent modulus of each fibre and the increments of axial deformation and curvature of the cross section.

The step-by-step evaluation of the stiffness parameters $\beta_{x,i}$, $\beta_{z,i}$, in accordance to Eqs. (68),(69), allows the updating of the *SDSF*s in Eqs. (56)-(61), the deformation matrix $\mathbf{B}(x; \beta_{x,i}, \beta_{z,i})$ in Eq. (78) and the element stiffness matrix $\mathbf{K}_e(\beta_{x,i}, \beta_{z,i})$ in Eq. (66). The smart character of these matrices allows the adoption of a single *SDB* element for each beam endowed with two *LRPD* devices able to capture the diffusion of plasticity along the inner portion avoiding any cumbersome sub-discretisation.

5 APPLICATIONS

The proposed *LRPDs*, optimized in accordance with the procedure presented in section 3, have been conceived, suitably inserted into steel frames, to obtain targeted push-over curves providing an equivalence between different structural systems. The above goal is implemented with numerical examples aiming at showing the successive phases of the procedure and to show the efficacy of the proposed smart beam element to model discontinuous cross section elements such as *LRPD* embedded into frame beam elements.

However, provisionally, single standing alone *LRPDs* have been analyzed with the specific aim of evaluating the internal stress distribution and assess the influence of stress concentration phenomena due to discontinuities between inner and outer portions. Precisely, for the latter cases, the accuracy of the smart beam element approach has been assessed in comparison to detailed 3D solid FEM models.

In particular, the case of a targeted *LRPD* designed for an IPE 270 shape for an $\alpha_{el} = 0.8$, sketched in Fig. 10 a), has been considered. The geometric characteristics of this *LRPD* are reported in Table 1.

Table 1 Results of the optimal design of *LRPD* for IPE 270 for an $\alpha_{el} = 0.8$ (dimensions in mm).

h^*	248.451
$t_{f,o}$	21.549
$t_{f,i}$	8.475
ℓ_o	80.062
ℓ_i	202.500
$t_{w,o}$	6.600
$t_{w,i}$	6.600

The material model is elastic-perfectly plastic with mechanical characteristics corresponding to an S235 steel grade. The model is clamped at one edge and endowed with a rigid plate on the other. The loading is represented by a pressure applied on the plate, linearly varying along the height, equivalent to a bending moment whose value ranges from 0 to the relevant M_{pl}. The latter *LRPD* has been modeled by means of 3D solid tetrahedral elements in ABAQUS environment with a corresponding adopted mesh size equal to 2 mm as sketched in Fig 10 b).

The von Mises stress maps are reported in Figs. 10 c)-d) for two different values of the acting bending moment. Examination of the latter figures shows the presence of boundary effects due to abrupt cross section changes but these effects do not influence the overall prescribed behavior of the device.

Other 3D FEM models of different *LRPD* have been analyzed by considering different cross section shapes (for complete details on the model as well as on the results see [5]) however, for brevity's sake, they are not reported in this paper.

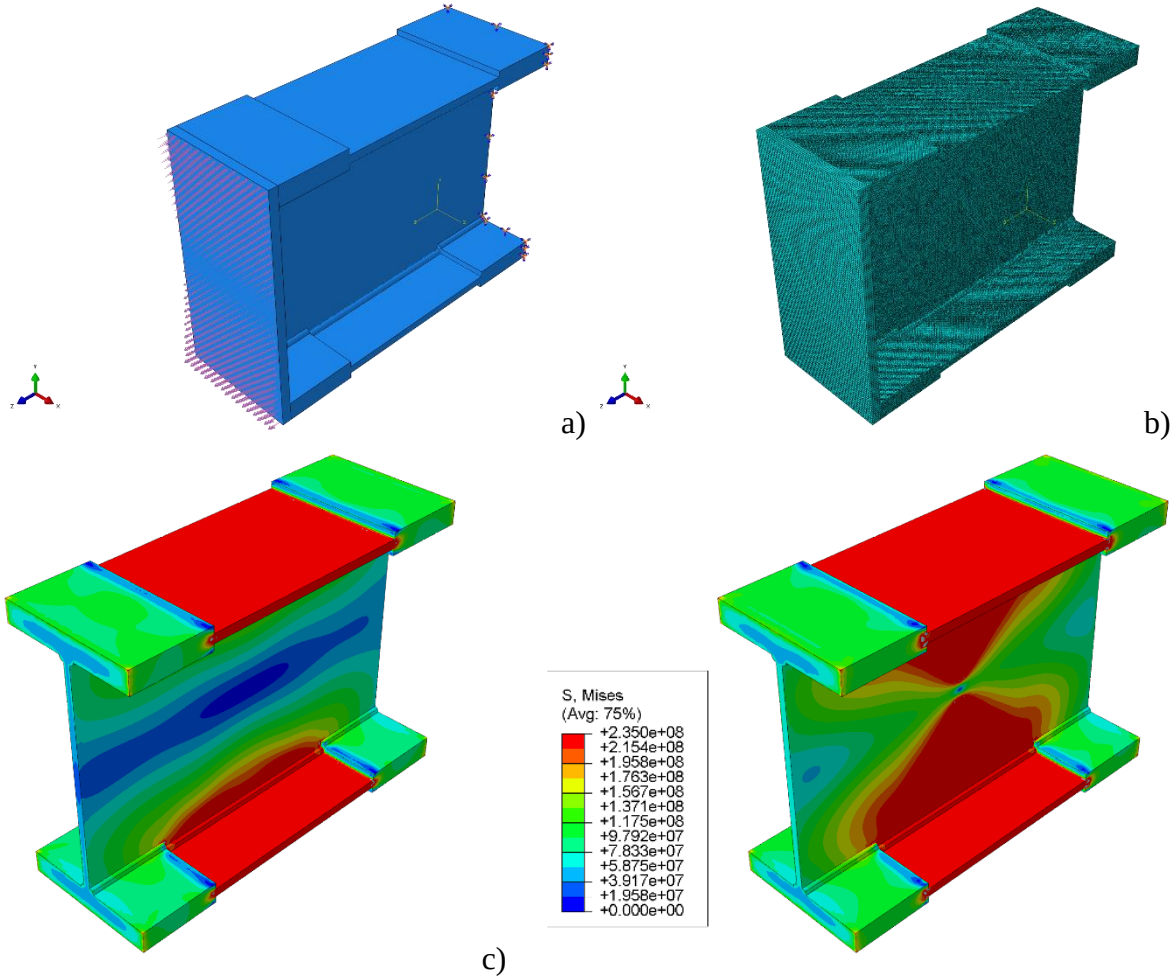


Figure 10. *LRPD* device designed for IPE 270 profile and $\alpha_{el} = 0.8$: a) 3D model; b) FE Mesh; c)-d) Von Mises stress maps [Pa] for M=57 kNm and M=91 kNm.

In order to check the reliability of the approach reported in section 4, the *LRPD* sketched in Fig. 10a) has been also modeled by means of a single smart beam element endowed with

7 Gauss points. The results, in terms of bending moment vs curvature are plotted in Fig. 11. In the same figure, the limit bending analysis of an IPE 270 beam, performed both in ABAQUS environment and by *FSDB* approach, is also reported with the principal aim of verifying that the limit behaviour of *LRPD* is the prescribed one (i.e. the limit bending moment is 80% of that of an IPE 270 profile).

An examination of this figure reveals that the proposed optimal design of *LRPD* is able to guarantee the prescribed limit behaviour and that proposed approach is able to correctly model the behaviour of a beam characterized by geometrical discontinuities with a very small error (<3%).

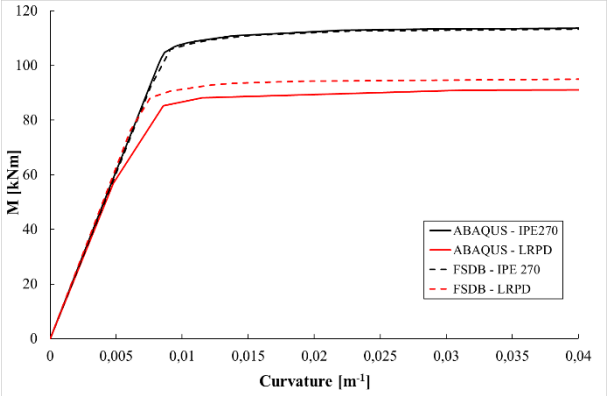


Figure 11. Comparison between FEM model (ABAQUS) and *FSDB* model (HISTRA) in terms of curvature-bending moment curves.

Once the reliability of the *FSDB* model has been assessed and the mechanical behaviour of the *LRPD* has been checked, the performance of the proposed design procedure of *LRPD* devices to be utilised in steel frames providing a nonlinear behaviour equivalent to given masonry walls is tested. The nonlinear behaviour of the frames endowed with *LRPD* devices is conveniently assessed by means of the use of the proposed *FSDB* beam element.

The first application concerns the design of a plane steel frame devoted to substitute a masonry panel and characterised by a nonlinear force-displacement response as similar as possible to the given masonry panel.

The considered masonry panel (denoted as Panel 1) is reported in Fig. 12 and its geometrical and mechanical features are reported in Table 2.

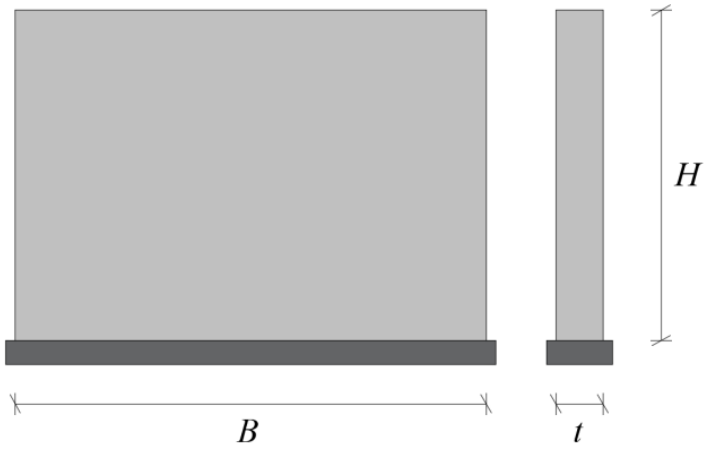


Figure 12. Panel 1: geometry.

Table 2. Masonry Panel 1: geometrical and mechanical features.

Geometric parameters		*Material parameters*	
B	5.00 m	*E*	1000 MPa
H	3.50 m	*G*	400 MPa
t	0.50 m	f_m	2.00 MPa
		f_{tm}	0.10 MPa
		f_{v0}	0.25 MPa

The masonry Panel 1 under study subjected to a constant distributed vertical load $q = 25$ kN/m and to an increasing horizontal concentrated load F, is reported in Fig. 13. The response has been obtained by means of a nonlinear incremental analysis conducted by imposing constant displacement increments of 1 mm at the top section of the panel. The numerical analyses have been performed by means of the software 3DMacro [49] by employing a discrete macro-element approach able to simulate the in-plane flexural and shear diagonal failure mechanisms of masonry panels. The adopted macro-element model consists in an assemblage of articulated quadrilaterals, simulating the masonry shear deformability, connected by interface elements, composed of a discrete distribution of nonlinear transversal links able to simulate the axial and flexural behaviour of masonry [50]. In the analyses, a single macro-element has been employed to simulate the entire panel while an interface element, endowed with nonlinear links, to simulate the axial and flexural behaviour of masonry and the interaction with the external base support has been adopted. A 150 mm interval between the nonlinear links of the interface has been assumed and for each f them an elasto plastic constitutive law has been adopted to simulate the masonry axial/flexural behaviour with fixed ductility capacity equal to 1.5 in tension and 3.0 in compression. The diagonal shear behaviour has been simulated by and elasto plastic constitutive law with Mohr-Coulomb yield criterion. The complete set of the mechanical parameters characterising the model is reported in Table 1 where, E and G are the Young's and shear moduli, f_m and f_{tm} the compression and tensile strengths, f_{v0} the shear strength in absence of axial load. Finally, a friction factor equal to 0.4 has been considered in Mohr-Coulomb criterion. The calibration procedures to evaluate the mechanical properties of the nonlinear links from the masonry properties are described in [51].

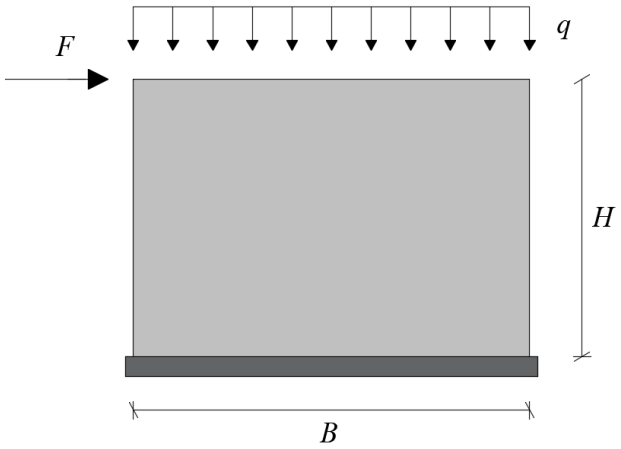


Figure 13. Panel 1: acting loads.

In the diagram of Fig. 14 the response in terms of displacement of the top of the panel vs shear force F (capacity curve) is reported. It is easy to observe that the panel exhibits a clear bilinear behaviour characterized by an initial elastic response up to the horizontal load level $F_{el} = 1{,}130$ kN and a subsequent response showing an horizontal displacement increment correspondent to an almost negligible load increment (the maximum observed value is $F_{max} = 1{,}180$ kN).

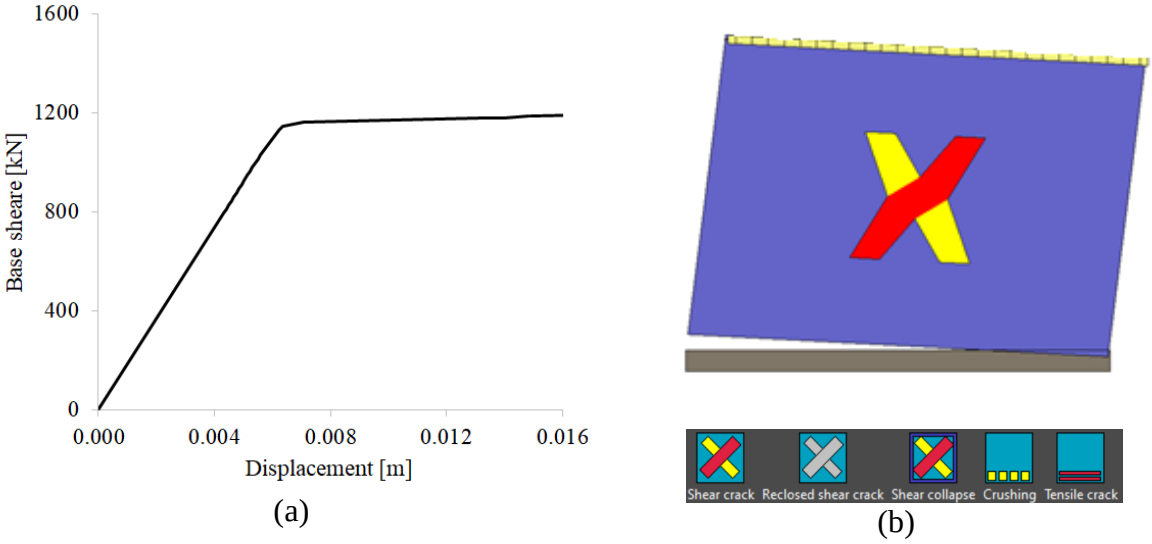
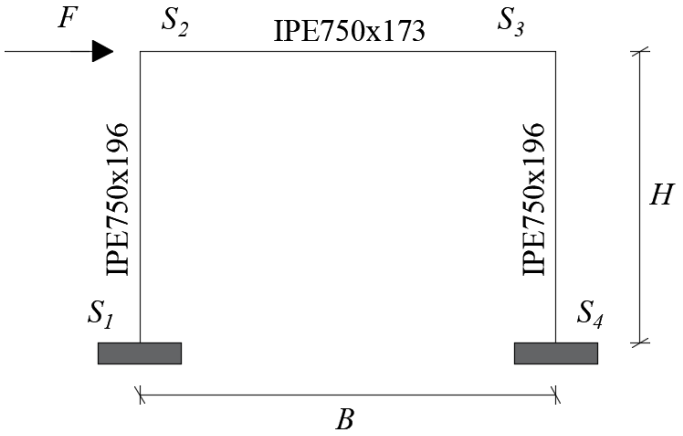


Figure 14. Panel 1: (a) capacity curve and (b) deformed shape at the last step.

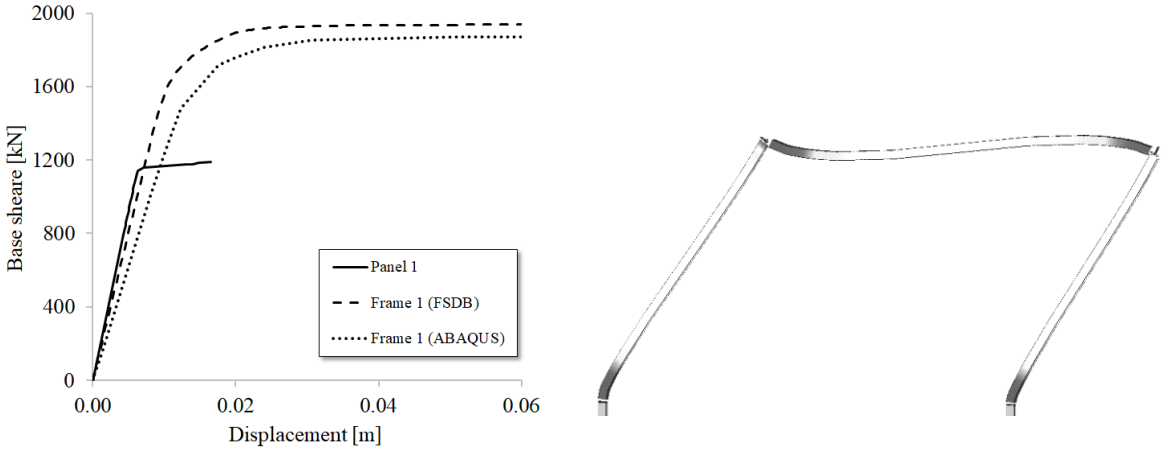
The steel plane frame (denoted as Frame 1), entitled to reproduce the nonlinear capacity curve of Panel 1, has been first designed by imposing an appropriate initial elastic stiffness as close as possible to the masonry panel stiffness by making use of standard steel profiles. On this basis, for Frame 1, IPE750×196 for the columns and IPE750×173 for the beam have been chosen (Fig. 15).

The nonlinear elastic-plastic analysis of Frame 1, assuming an S235 steel grade, has been conducted by means of the *FSDB* model proposed in [29] through the software HiStrA [52] where the model has been implemented. A single finite element has been employed to simulate each frame element. The Gauss-Lobatto integration scheme with 10 integration points, uniformly distributed along the element length, has been adopted. Finally, the beam element Gauss-Lobatto cross sections have been discretised by means of 40 fibres.



735 Figure 15. Frame 1: geometry and load condition.

736 In Fig. 16a the complete horizontal force-top displacement diagram of Frame 1, together
737 with the analogous diagram of Panel 1, is reported. In the same figure the results obtained by
738 modelling Frame 1 in ABAQUS environment are also reported as benchmark. The ABAQUS
739 model is characterized by 3D tetrahedral elements, with an adopted mesh size equal to 10
740 mm, and an S235 steel grade with an elastic perfectly plastic mechanical behaviour. From
741 Fig. 16a it can be observed that the initial elastic stiffness of Frame 1, both in the case of
742 *FSDB* and in ABAQUS models, is slightly lower than the one which characterizes the
743 masonry Panel 1. The reason of such behaviour lies on the choice made for standard
744 commercial profiles whose geometric characteristics do not allow to exactly reproduce the
745 initial elastic stiffness. Another important remark regards the differences of the results
746 between the *FSDB* and the ABAQUS models. These differences have to be ascribed to the
747 fact that the *FSDB* model is based on the Euler-Bernoulli beam theory while the ABAQUS
748 one is based on 3D solid elements. On the other hand, as expected, the resistance capacity of
749 the steel frame in both models is much higher than the analogous quantity related to Panel 1.
750 In figure 16b, the deformed shape of the frame at 20 mm displacement is reported. The
751 distribution of the $\beta_{z,i}, i = 1, \dots, n_G$ parameters is also reported in Fig. 16b through a
752 grayscale color map, set according to [29].



753 Figure 16. Capacity curve comparison.

754 To our purpose, namely a plane steel frame design exhibiting a force-displacement
755 behaviour as close as possible to the masonry panel, the *LRPD* devices have been favourably
756 utilised. It is worth noting that employment of *LRPD* devices, as described in section 3,
757 allowed an appropriate frame design characterised by assigned initial elastic stiffness and
758 prefixed limit resistance capacity, both features being independent of each other.
759 A preliminary fundamental step, prior to performing the design of the *LRPD* equipped
760 frame, consisted in selecting the number and positions of the devices. In the present
761 application four *LRPD* placed at the base of the columns and at the extreme cross sections of
762 the beam, as depicted in Fig. 17, have been chosen.
763

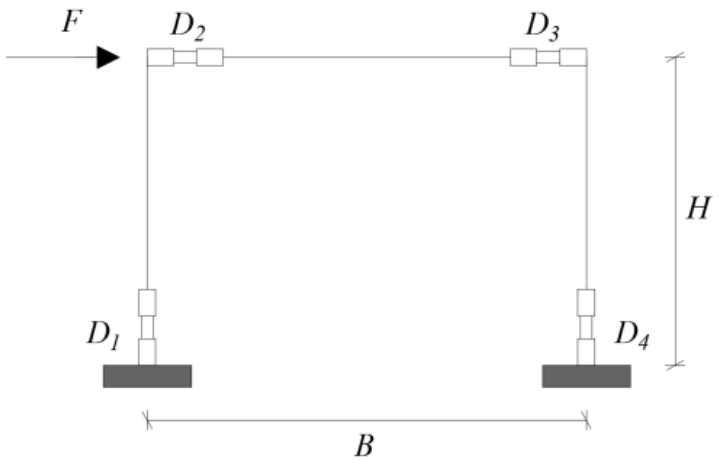


Figure 17. *LRPD* insertion scheme for Frame 1.

In view of the bilinear shape of the diagram reported in Fig. 14 for Panel 1 to be reproduced, all the *LRPD* devices have been imposed to reach the requested limit resistance for the same external load level. The chosen external load limit intensity is $F_{lim} = 1{,}150$ kN, that represents an appropriate mean value characterizing the upper plateau of the relevant Panel 1 diagram. The elastic response of the steel frame without the *LRPD* and subjected to the indicated load is reported in Fig. 18 in terms of axial force, shear force and bending moment.

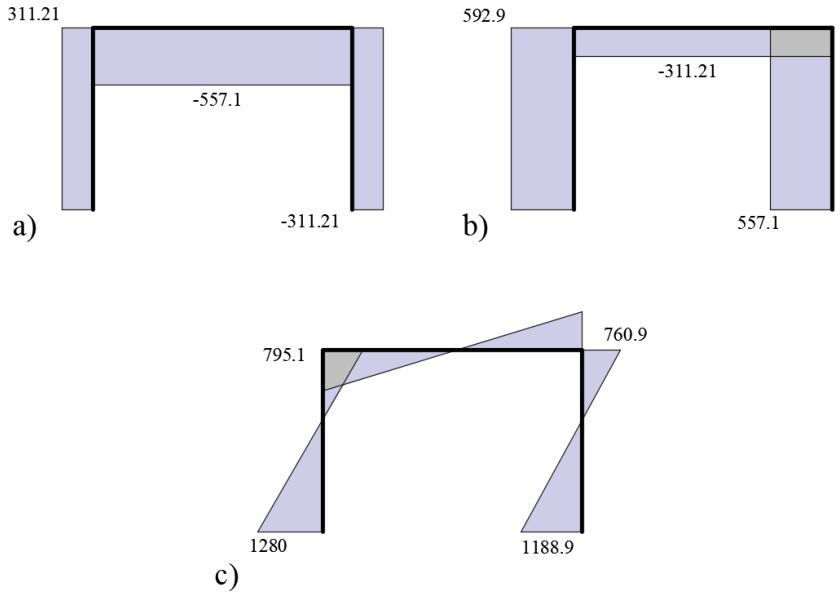


Figure 18. Frame 1 response: a) axial force (kN); b) shear force (kN); c) bending moment (kNm).

The optimal design of the four devices has been obtained as the solution to the problem defined by Eqs. (26)-(30), whose data are reported in Table 3, by utilizing the Matlab Optimization toolbox that provides solvers for the numerical solution of non-linear minimization problems. In particular, the "fmincon" solver is utilized by adopting an interior-point algorithm.

Table 3. Geometrical and mechanical data for *LRPD* designs.

	device D_1	device D_2	device D_3	device D_4
β	0.5	0.5	0.5	0.5
$H = h$ [mm]	770	762	762	770
b [mm]	268	267	267	268
$t_{f,p}$ [mm]	25.4	21.6	21.6	25.4
$t_{w,p}$ [mm]	15.6	14.4	14.4	15.6
α_{tp}	0.614	0.67	0.67	0.614
N_a [kN]	311.21	-557.1	-557.1	-311.21
$M(0)$ [kNm]	1,280	795.1	760.9	1,188.9
T [kN]	592.9	-311.21	-311.21	557.1
f_y [MPa]	235	235	235	235
I_p [cm^4]	240,300	205,800	205,800	240,300

The results of the reached optimal designs are reported in Table 4. The complete nonlinear analysis of Frame 1 equipped with the four optimal *LRPD* devices has been conducted by means of the assemblage of three (two columns and one beam) *SDB* beam elements proposed in section 4. Furthermore, the beam element Gauss cross sections, chosen as in Fig. 7, have been discretised by means of 40 fibres each.

In Fig. 19 the shear force vs top displacement diagram representing the nonlinear response of the frame equipped with the optimal *LRPD* devices obtained by *FSDB* model is reported and compared with the diagram of the given Panel 1 and with that obtained in ABAQUS environment suitably modelling by 3D tetrahedral elements the frame equipped with the four optimal *LRPD* devices, adopting a mesh size equal to 10 mm for the beam and 2 mm for the devices, and an S235 steel grade with an elastic perfectly plastic mechanical behaviour. The comparison between the sketched diagrams clearly shows the effectiveness of the computational approach and the reliability of the utilised devices.

Table 4. *LRPD* optimal geometry [mm].

	D_1	D_2	D_3	D_4
h^*	709.97	710.68	710.34	705.49
$t_{f,o}$	60.03	51.33	51.67	64.51
$t_{f,i}$	15.38	10.64	10.51	13.60
ℓ_o	315.24	449.45	458.32	398.10
ℓ_i	385.00	381.00	381.00	385.00
$t_{w,o}$	33.81	31.67	31.85	35.87
$t_{w,i}$	8.75	6.60	6.52	7.65

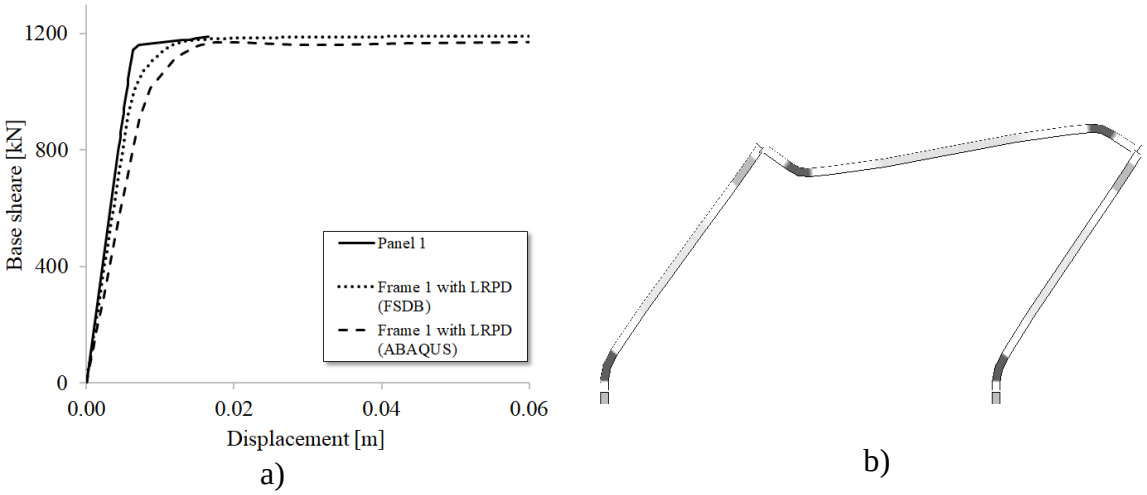


Fig. 19. Frame with *LRPD* device: a) capacity curve and b) deformed shape at 20mm with plastic zones.

To further demonstrate the wide applicability of the proposed computational approach and the practical utilisation of the proposed devices in structural engineering an additional application is reported in what follows.

This second application concerns the design of a plane steel frame devoted to substitute a masonry panel (denoted as Panel 2) in presence of an opening. The considered masonry panel is sketched in Fig. 20 and in Tab. 5 its geometrical and mechanical features are reported.

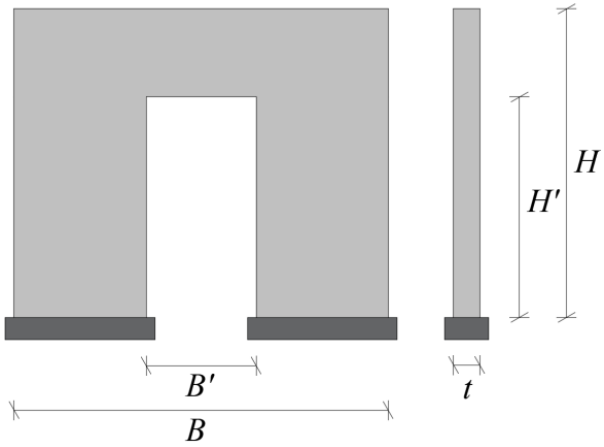


Figure 20. Panel 2: geometry.

Table 5. Panel 2: geometrical and mechanical features.

B/B'	4.25/1.25 m	*G*	550 MPa
H/H'	3.5/2.5 m	f_m	2.60 MPa
T	0.30 m	f_{tm}	0.10 MPa
E	1250 MPa	f_{v0}	0.25 MPa

The masonry Panel 2 subjected to a constant distributed vertical load $q = 125$ kN/m and an increasing horizontal concentrated load F, is reported in Fig. 19a. The panel has been analysed in accordance to a macro-element approach [50]-[51] and, in particular, it has been discretised by means of five macro-elements, with the relevant interfaces, as depicted in Fig.

21b. The response has been obtained by means of a nonlinear incremental analysis performed by means of the software 3DMacro [54] and conducted by imposing constant displacement increments of 0.25 mm at the top section of the panel.

An elastic plastic constitutive law has been adopted to simulate the masonry axial/flexural behaviour, concentrated at the interfaces, with fixed ductility capacity equal to 1.5 in tension and 3.0 in compression. The diagonal shear behaviour modelled by means of the macro-elements has been simulated by means of an elastic plastic constitutive law with Mohr-Coulomb yield criterion. The complete set of the mechanical parameters characterising the model is reported in Table 5 where, E and G are the Young's and shear moduli, f_m and f_{tm} the compression and tensile strengths, f_{v0} the shear strength in absence of axial load. Finally, a friction factor equal to 0.4 is considered in Mohr-Coulomb criterion.

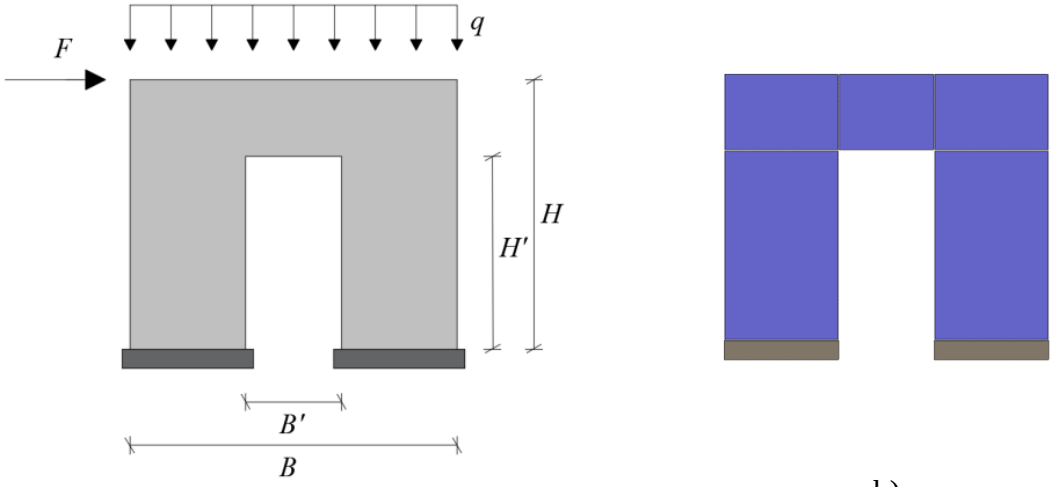


Figure 21. Panel 2: a) acting loads; b) macro-element discretisation.

In Fig. 22 the nonlinear response of Panel 2 in terms of top displacement vs shear force is reported. Differently from the first application, this panel exhibits a very smooth behaviour characterised by an initial elastic response till the horizontal load reaches the value $F_{el} = 95$ kN and a subsequent smooth nonlinear behaviour asymptotically converging to $F_{max} = 180$ kN.

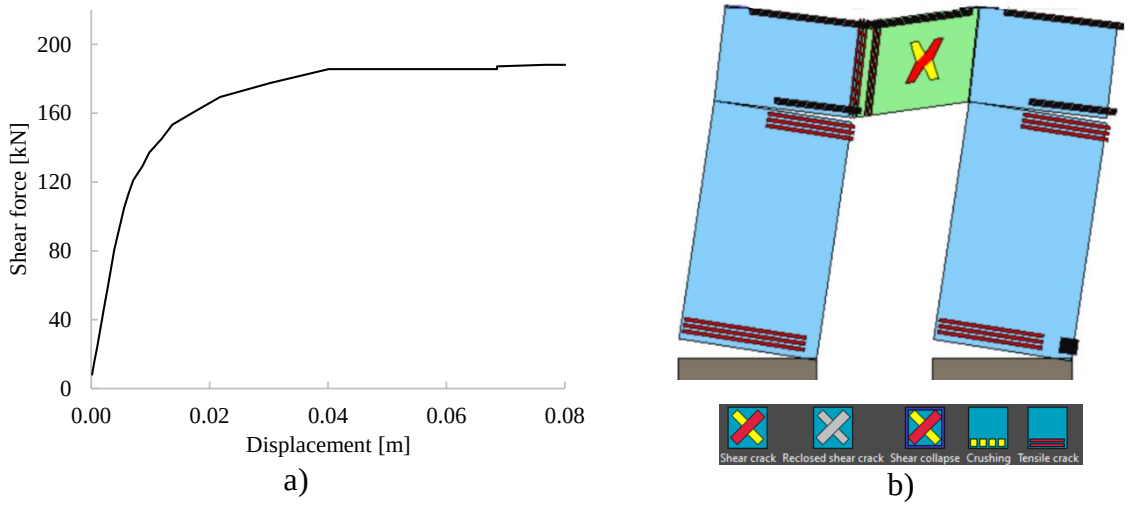


Figure 22. Panel 2: Panel 2: a) capacity curve and b) deformed shape at 8mm displacement.

The standard steel profiles constituting the portal frame (denoted as Frame 2) replacing the masonry Panel 2, have been chosen by imposing an initial elastic stiffness as similar as possible to the panel one as follows: IPE400 for the columns and IPE360 for the beam (Fig. 23).

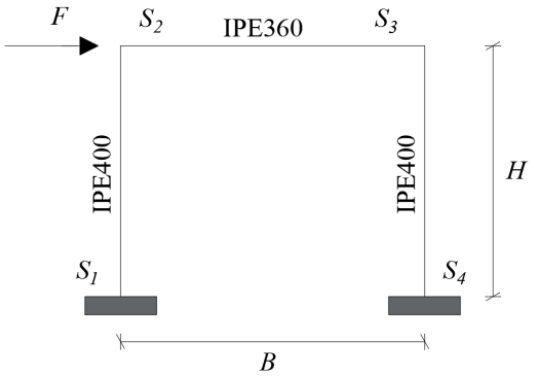


Figure 23. Frame 2: geometry and load condition.

The nonlinear elastic-plastic analysis of Frame 2 has been conducted by means of the *FSDB* model [29] implemented in the structural code HiStrA [52]. For each finite element 10 integration points and the Gauss-Lobatto integration scheme have been considered. The cross sections subjected to integration of the elastic plastic constitutive laws have been discretised with 40 fibres. Also for Frame 2 the check of the reliability of the *FSDB* model to reproduce the frame behaviour, has been performed by suitably modelling in ABAQUS environment adopting 3D solid tetrahedral element, an S235 steel grade with an elastic perfectly plastic mechanical behaviour with an adopted mesh size equal to 10 mm (see Fig. 24).

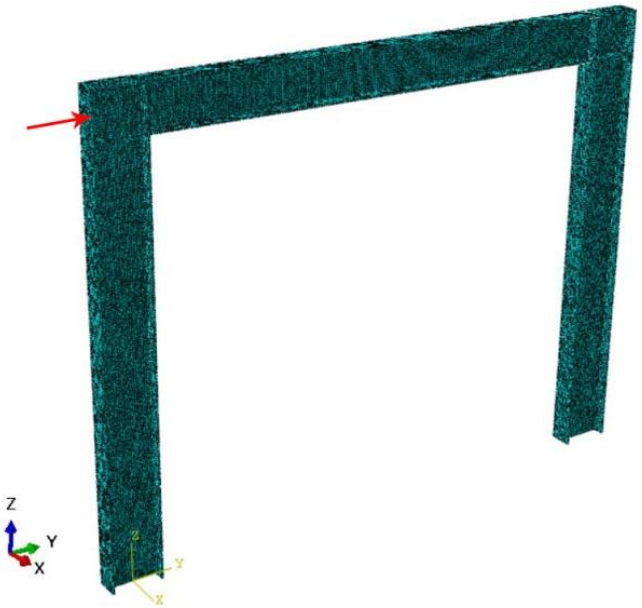


Figure 24. Frame 2 modelled in ABAQUS environment.

In Fig. 25 the complete diagram force-displacement of the steel Frame 2 together with the analogous diagram of the original masonry Panel 2 and that obtained by pushover analysis in ABAQUS are reported.

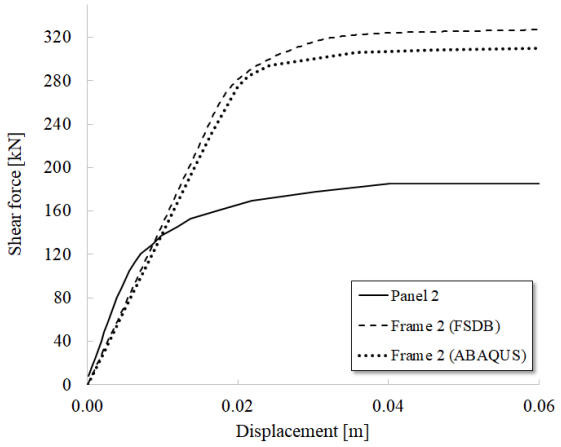


Figure 25. Capacity curve comparison of the Frame 2.

From Fig. 25 it can be observed that, in view of the choice of standard commercial profiles, the initial elastic stiffness of the frame is slightly lower of the Panel 2 and the resistance capacity of the steel frame is much higher than the masonry panel one. The comparison between the curves obtained by *FSDB* model and ABAQUS reveals that, as it could be expected, the results, in terms of stiffness and ultimate load, from *FSDB* model (based on the Euler-Bernoulli beam) are slightly different from those obtained from 3D FEM analysis but it confirms the reliability of the *FSDB* model.

Modification of the capacity curve of Frame 2 has been pursued by means of the optimal design of *LRPD* devices suitably inserted at pre-selected positions. Precisely, the devices have been inserted at the base of the columns and at the extreme cross sections of the beam. Due to the smooth shape of the diagram to be respected, an appropriate sequence of plastic activation for the *LRPD* had to be imposed.

In particular, making reference to the masonry Panel 2 diagram in Fig. 22, the optimal design of the devices has been found by solving to the problem defined by Eqs. (26)-(30), considering the load intensity levels reported in Table 6:

Table 6. Load levels for *LRPD* designs.

	Load level [kN]
device D_1	F_1 = 95
device D_2	F_2 = 150
device D_3	F_3= 180
device D_4	F_4 = 95

i.e. by imposing the plasticization of the devices D_1 and D_4 for the first load intensity level $F_1 = F_4 = 95\,kN$, the plasticization of the device D_2 for $F_2 = 150\,kN$ and the ultimate resistance capacity, correspondent to fully plastic behaviour of device D_3, for the highest load intensity level $F_3 = 180\,kN$.

In order to perform the optimal design of the *LRPD* devices according to Eqs. (26)-(30) the responses of the frame to the above listed load intensities have been preliminarily and

approximately evaluated. The latter analyses have been conducted by means of successive linear analyses in accordance to a rigid plastic hinge behaviour of the devices depending on the progressive plastic activation sequence ($D_1, D_4 \Rightarrow D_2 \Rightarrow D_3$). Precisely, the response in terms of axial force, shear force and bending moment depicted in Figs. 26, 27 and 28 had to be considered

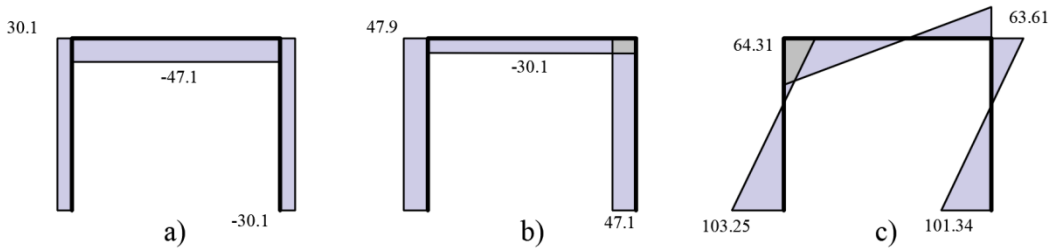


Figure 26. Frame 2 elastic response for load level $F = F_1$: a) axial force (kN); b) shear force (kN); c) bending moment (kNm).

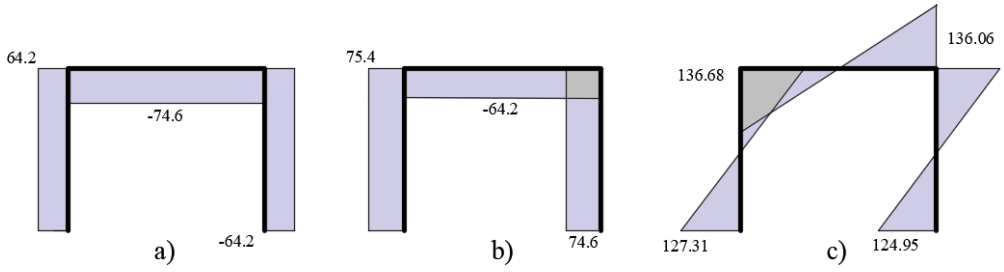


Figure 27. Frame 2 response with devices D_1, D_4 active for load level $F = F_2$: a) axial force (kN); b) shear force (kN); c) bending moment (kNm).

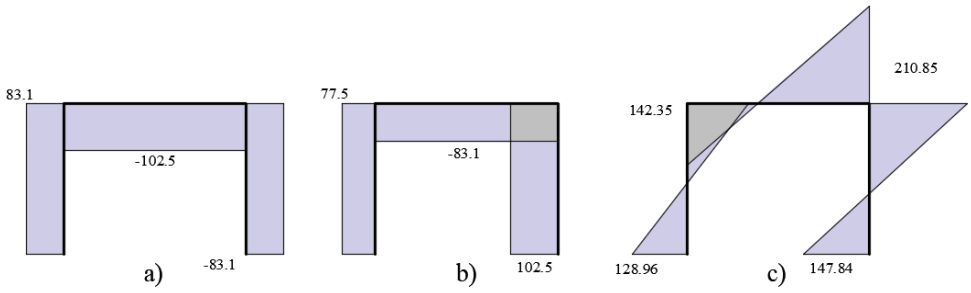


Figure 28. Frame 2 response with device D_1, D_4, D_2 active for load level $F = F_3$: a) axial force (kN); b) shear force (kN); c) bending moment (kNm).

together with the further data reported in Table 7:

Table 7: Geometrical and mechanical data for *LRPD* designs.

	device D_1	device D_2	device D_3	device D_4
β	0.5	0.5	0.5	0.5
$H = h$ [mm]	400	360	360	400
b [mm]	180	170	170	180
$t_{f,p}$ [mm]	13.5	12.7	12.7	13.5
$t_{w,p}$ [mm]	8.6	8.0	8.0	8.6

α_{tp}	0.637	0.59	0.59	0.637
N_a [kN]	30.1	-74.6	-102.5	-30.1
$M(0)$ [kNm]	103.25	136.68	210.85	101.34
T [kN]	47.9	-64.2	-83.1	47.1
f_y [MPa]	235	235	235	235
I_p [cm^4]	23,130	16,270	16,270	23,130

The optimal results obtained by solving the problem defined by Eqs. (26)-(30) always by means of the "fmincon" solver available in Matlab Optimization toolbox are reported in Table 8.

Table 8. *LRPD* optimal geometry [mm].

	D_1	D_2	D_3	D_4
h*	368.39	331.69	337.56	368.20
$t_{f,o}$	31.61	28.31	22.44	31.80
$t_{f,i}$	6.55	6.74	12.52	6.40
ℓ_o	290.57	224.22	31.52	301.29
ℓ_i	200.00	180.00	180.00	200.00
$t_{w,o}$	17.58	15.84	12.95	17.67
$t_{w,i}$	3.67	3.80	7.24	3.59

The complete nonlinear analysis of Frame 2 equipped with the four optimal *LRPD* devices reported in Table 7 has been conducted by means of the assemblage of four *SDB* beam elements proposed in section 4 where the beam element Gauss cross sections, chosen as in Fig. 7, have been discretised by means of 40 fibres each.

In Fig. 29 the diagram shear force vs displacement representing the response of Frame 2 equipped with the optimal *LRPD* devices is reported together with the analogous diagram referred to Panel 2. The comparison between the sketched diagrams clearly shows the effectiveness of the computational approach and the perfect reliability of the utilized devices.

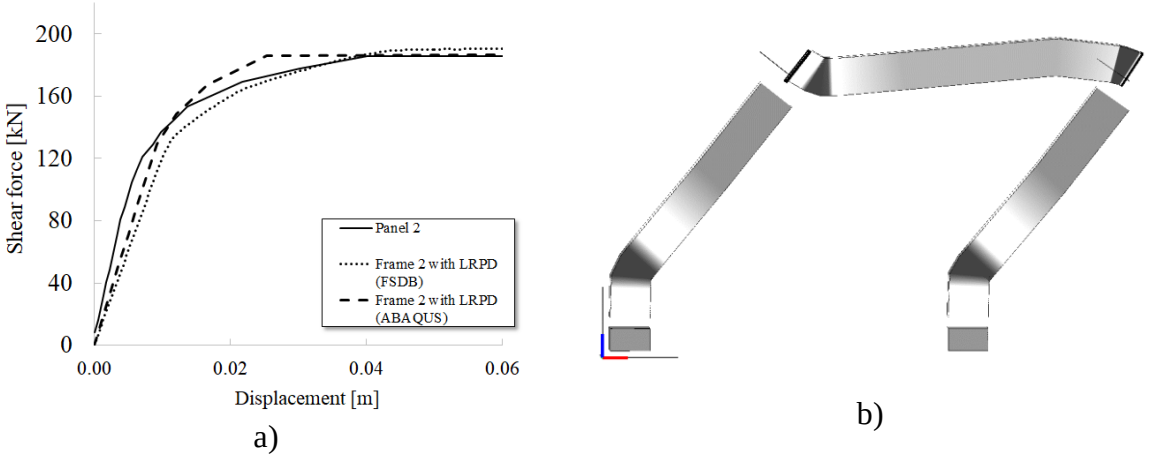


Figure 29. Frame 2 with *LRPD* devises: (a) capacity curve comparison; (b) ultimate deformed shape.

It is clear that different positions of the devices or different sequence of their activation involve different behaviour of the frame. As an example, two additional frames have been designed. The first one is related to a model in which all the devices are designed to activate

simultaneously for the maximum expected horizontal load ($F_{max} = 180$ kN), providing a bilinear like behaviour. The second one is related to a model in which the devices at the base of the columns activate simultaneously for the elastic limit load ($F_{el} = 95$ kN) and the devices at the ends of the beam for the maximum expected shear force ($F_{max} = 180$ kN), providing a trilinear like behaviour.

In Fig. 30 the response of the latter two additional frames in comparison with the response of the masonry Panel 2 and of the original equivalent Frame 2 (quadri-linear curve) are reported. Fig. 30 shows great influence of the *LRPD* design on the structural behaviour and, ultimately, the efficacy of the proposed *LRPD* equipment with respect to different choices and the great adaptability of the proposed intervention to the structural demand.

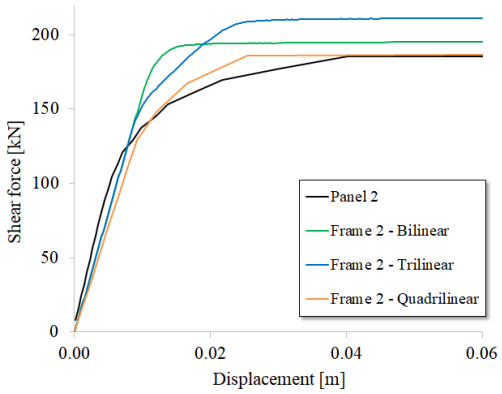


Fig. 30: Capacity curves comparison for different design approaches.

6 CONCLUSIONS

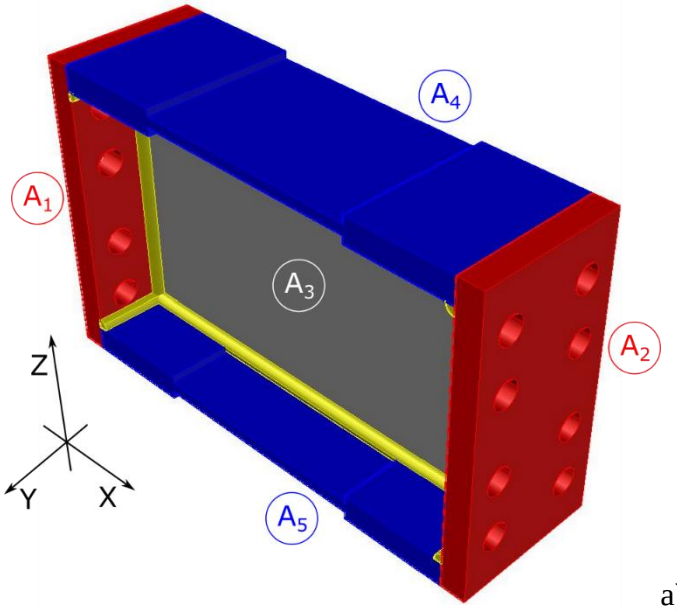
The present paper proposed a new approach in the design of steel frames aimed at reproducing a pre-established target push-over curve which is a common structural problem when a masonry wall is substituted by a steel frame. The proposed approach is characterized by two different phases. In the first one, the Limited Resistance Plastic Device (*LRPD*) is proposed as fundamental tool to govern the structural response of the frame to reproduce as close as possible the target push-over curve. The *LRPD* is a stepped cross section device to be inserted along selected structural members possessing two main specific features: i) any elastic flexural stiffness variation of the original selected member must be avoided; ii) an ultimate plastic bending moment value equal to an assigned percentage of the original limit resistance value must be ensured. The geometric characteristics of the *LRPD* are obtained by a new suitably defined optimal design also reported in the paper. The second phase is that of obtaining the structural response of the frame equipped with one or several *LRPDs* which are characterized by structural element with discontinuous geometric characteristics. To reach this goal in the paper an extension of a recently proposed Fibre Smart Displacement Based (*FSDB*) beam element model, characterized by the adoption of updating shape functions has been adopted.

The first step in the application of the proposed approach has been the test of the real behaviour of the *LRPD* as well as the check of the efficacy of *FSDB* element in correctly modelling the response of a structural element with discontinuous geometric characteristics. The obtained results have been compared with those arising from a 3D FEM analyses in ABAQUS environment. The second step in the application has been to perform the design of two plane steel frames, equipped with *LRPD*, replacing two different masonry panels, imposing that the frames exhibit the same elastic behaviour and limit resistance of the given masonry

panels. Even in this second step the obtained results have been validated against detailed 3D finite element models. The obtained results confirm the great reliability of the *LRPD* devices to design structures with prescribed mechanical characteristics as well as the efficacy and the feasibility of the numerical modelling by means of *FSDB* beam elements. Indeed, the application of the proposed specialized *FSDB* beam element model allowed the description of the real behaviour of the *LRPD* in the field of distributed plasticity.

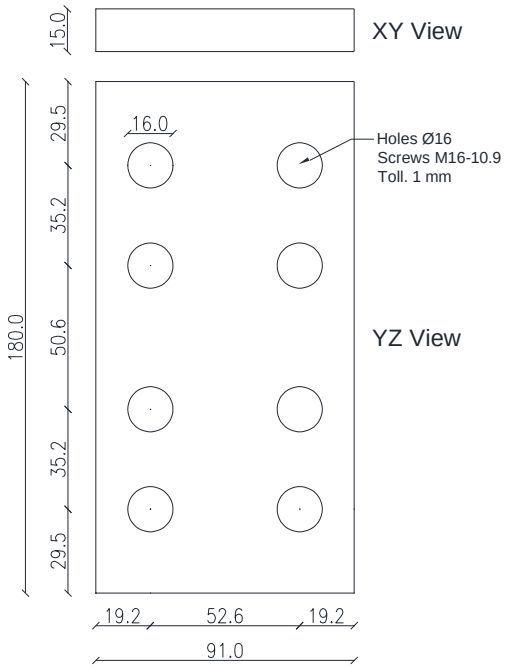
APPENDIX

In this appendix all the information required to realize the *LRPD* device are reported. These information are for a *LRPD*, designed for a IPE180 profile, produced by the Tecnozinco srl industry whose support in this research is gratefully acknowledged.
Basically, *LRPD* are composed by five different parts and they are indicated from A_1 to A_5 in Fig. 30 a) where a 3D view of the assembly is sketched. Part A_1 and A_2, sketched in Fig. 30 b), are identical and they play the role of connection plates with the structural element (to this aim in Fig. 30 b) the holes for the screws are indicated); part A_3, sketched in Fig. 30 c), is realized from a single plate of suitable thickness by milling and it represents the web of *LRPD*; parts A_4 and A_5, sketched in Fig. 30 d), are identical, each part is realized from a single plate of suitable thickness by milling and it represents one flange of *LRPD*. As it is easy to observe by an examination of Fig. 30 a), the assembly of *LRPD* imposes welding between parts (indicated in light yellow in Fig. 30 a)) in order to realize the device. The welding adopted at this stage of the research is a fully penetration one.



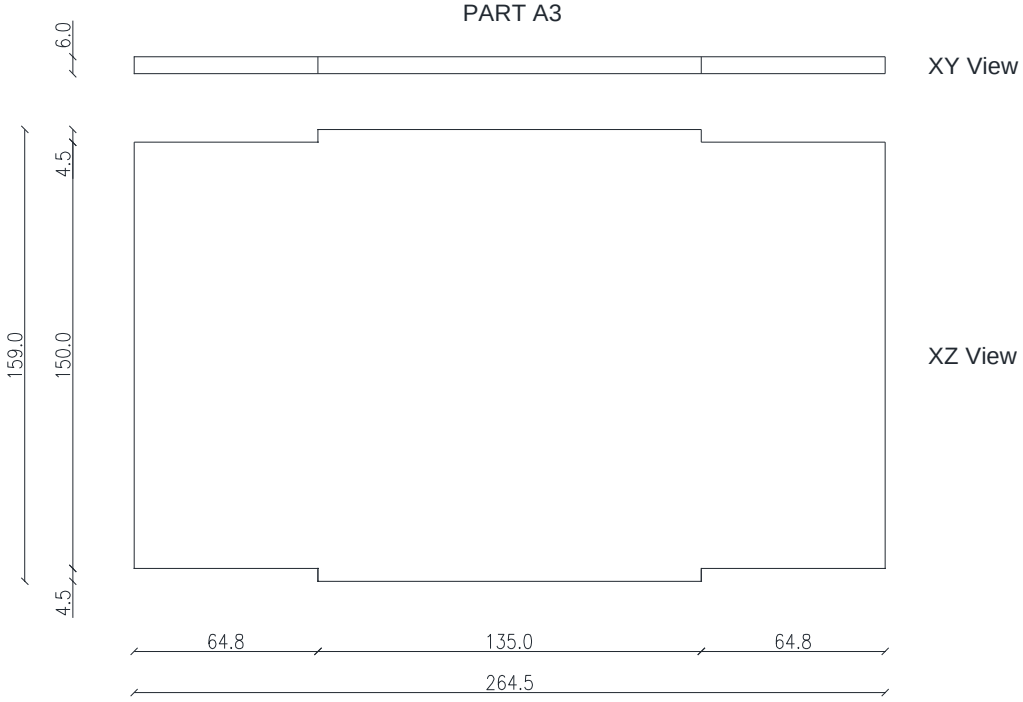
a)

PARTS A1-A2

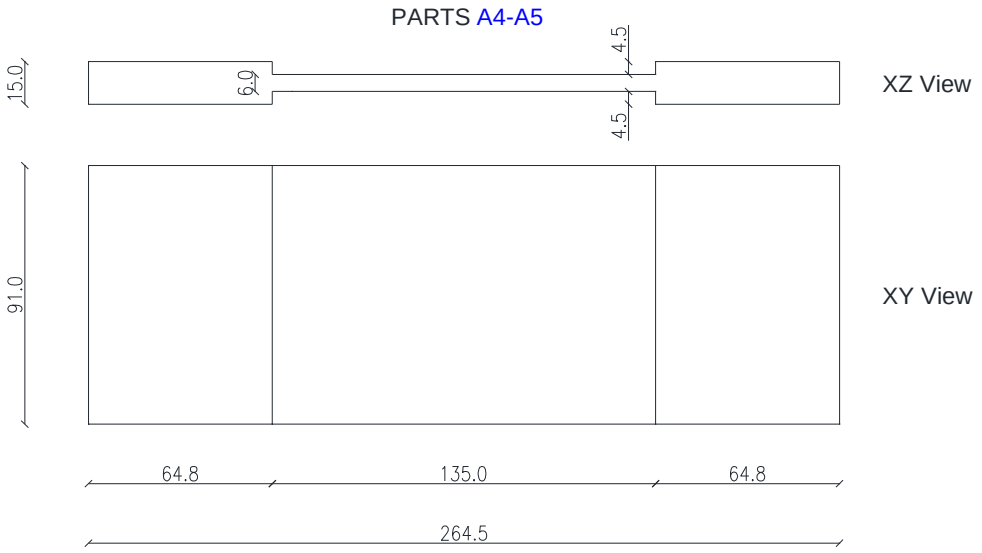


975 b)

PART A3



976 c)



d)

Fig. 30: Technical drawings of *LRPD* (dimensions in mm): a) 3D view of the assembly; b) parts A1-A2; c) part A3; d) parts A4-A5.

REFERENCES

[1] S. Benfratello, C. Cucchiara, L. Palizzolo, P. Tabbuso, Fixed Strength And Stiffness Hinges For Steel Frames. *Proceedings of the 23rd Conference of the Italian Association of Theoretical and Applied Mechanics (AIMETA 2017)*, Salerno, September, in Gechi Edizioni (Milano), **3**, 1287-1296, 2017.

[2] S. Benfratello, L. Palizzolo, Limited Resistance Rigid Perfectly Plastic Hinges for Steel Frames. *International Review of Civil Engineering*, **8**(6), 286-298, 2017.

[3] S. Benfratello, L. Palizzolo, P. Tabbuso, Optimal design of new steel connections. H. C. Rodrigues et al. (Eds.): *EngOpt 2018 Proceedings of the 6th International Conference on Engineering Optimization*, 644–656, 2019.

[4] S. Benfratello, L. Palizzolo, P. Tabbuso, S., Vazzano, On the post-elastic behavior of *LRPH* connections. *International Review on Modelling and Simulations*, **12**(6), 341-353, 2019.

[5] L. Palizzolo, S. Benfratello, P. Tabbuso, S. Vazzano, Numerical validation of *LRPH* behaviour by fem analysis, *Advances in Engineering Materials, Structures and Systems: Innovations, Mechanics and Applications - Proceedings of the 7th International Conference on Structural Engineering, Mechanics and Computation, 2019*, 2019, 1224-1229.

[6] S. Benfratello, L. Palizzolo, P. Tabbuso, S. Vazzano, *LRPH* device optimization for axial and shear stresses. *International Review of Civil Engineering*, **11**(4),152-163, *2020*.

[7] N.R. Iwankiw, C.J. Carter, The dogbone: a new idea to chew on. *Mod. Steel Constr.* **36** (4), 18-23, 1996.

[8] A. Plumier, The dogbone: back to the future. *Engineering Journal*, **34**(2), 61-67, 1997.

[9] J. Shen, T., Kitjasateanphun, W., Srivanich, Seismic performance of steel moment frames with reduced beam sections. *Engineering Structures*, **22**(8), 968-983, 2000.

[10] S. Wilkinson, G. Hurdman, A. Crowther, A moment resisting connection for earthquake resistant structures, *J. Constr. Steel Res.*, **62** (3), 295-302, 2006.

[11] J. Jin, S. El-Tawil, Seismic performance of steel frames with reduced beam section connections. *Journal of Constructional Steel Research*, **61**(4), 453-471, 2005.

[12] R. Montuori, The Influence of Gravity Loads on the Seismic Design of RBS Connections. *The Open Construction and Building Techn. J.*, **8** (Suppl 1:M6), 248-261, 2014.

[13] C.E. Sofias, C.N. Kalfas, D.T., Pachoumis, Experimental and FEM analysis of reduced beam section moment endplate connections under cyclic loading. *Eng. Str.*, **59**, 320-329, 2014.

[14] S. Momenzadeh, M.T., Kazemi, M.H., Asl, Seismic Performance of Reduced Web Section Moment Connections. *Int. Journal of Steel Structures*, **17**(2), 413-425, 2017.

[15] M.A. Morshedi, K.M., Dolatshahi, S., Maleki, Double reduced beam section connection. *Journal of Constructional Steel Research*, **138**, 283-297, 2017.

[16] FEMA-350, Recommended Seismic Design Criteria for New Steel Moment-Frame Buildings, 2000

[17] ANSI/AISC 358-16, Prequalified Connections for Special and Intermediate Steel Moment Frames for Seismic Applications, including Supplement No. 1, 2016

[18] K.J. Bathe, Finite Element Procedures, Prentice Hall, Englewood Cliffs, NJ, USA, 1996.

[19] M.A. Crisfield, Non-Linear Finite Element Analysis of Solids and Structures, vol.1, John Wiley & Sons, Chichester, UK, 1991.

[20] M.A. Crisfield, Non-Linear Finite Element Analysis of Solids and Structures, vol.2, John Wiley & Sons, Chichester, UK, 1997.

[21] O.C. Zienkiewicz, R.L. Taylor, The Finite Element Method: Solid Mechanics, vol.2, fifth ed., Butterworth-Heinemann, Oxford, UK, 1987.

[22] O.C. Zienkiewicz, R.L. Taylor, The Finite Element Method: The Basis, vol. 1, fifth ed., Butterworth-Heinemann, Oxford, UK, 2000.

[23] E. Spacone, V. Ciampi, F.C. Filippou, A Beam Element for Seismic Damage Analysis, Report No. UCB/EERCC-92/07 Earthquake Engineering Research Center, College of Engineering, University of California, Berkeley, 1992.

[24] E. Spacone, V. Ciampi, F.C. Filippou, Mixed formulation of nonlinear beam finite element, *Comput. Struct.*, **58** (1), 71–83, 1996.

[25] E. Spacone, F.C. Filippou, F.F. Taucer, Fiber beam–column model for non-linear analysis of r/c frames: Part I. Formulation, *Earthq. Eng. Struct. Dyn.*, **25**, 711–725, 1996.

[26] E. Spacone, F.C. Filippou, F.F. Taucer, Fiber beam–column model for non-linear analysis of r/c frames: Part II. Applications, *Earthq. Eng. Struct. Dyn.*, **25**, 727–742, 1996.

[27] F.F. Taucer, E. Spacone, F.C. Filippou, A Fiber Beam–Column Method for Seismic Response Analysis of Reinforced Concrete Structures, Report No. UCB/EERCC-91/17 Earthquake Engineering Research Center, College of Engineering, University of California, Berkeley, 1991.

[28] B. Pantò, D. Rapicavoli, S. Caddemi, I. Caliò, A smart displacement based (*SDB*) beam element with distributed plasticity, *App. Math. Model.*, **44**, 336-356, 2017.

[29] B. Pantò, D. Rapicavoli, S. Caddemi, I. Caliò, A Fibre Smart Displacement Based (*FSDB*) beam element for the nonlinear analysis of reinforced concrete members, *International Journal of Non-Linear Mechanics*, **117**, 103222, 2019.

[30] S. Benfratello, S. Caddemi, L. Palizzolo, B. Pantò, D. Rapicavoli, S. Vazzano "Smart beam element approach for *LRPH* device", Proceedings of the XXIV Conference The Italian Association of Theoretical and Applied Mechanics AIMETA'2019, Rome, Italy, 15-19 September 2019.

[31] EN 1993-1-8:2006, Eurocode 3: Design of Steel Structures Part 1-8: Design of Joints, 2006.

[32] Italian Ministry of Infrastructure and Transport, National Standard NTC 2018, DM 17/01/2018.

[33] EN 1993-1-5:2019, Eurocode 3: Design of Steel Structures Part 1-5: Plated structural elements, 2019.

[34] B.A. Izzudin, A.S. Elnashai, Adaptive space frame analysis: Part I, a plastic hinge approach, *Struct. Build.*, **99** (3), 303–316, 1993.

[35] B.A. Izzudin, A.S. Elnashai, Adaptive space frame analysis: Part II, a distributed plasticity approach, *Struct. Build.*, **99** (3), 317–326, 1993.

[36] B.A. Izzudin, C.G. Karayannis, A.S. Elnashai, Advanced nonlinear formulation for reinforced concrete beam–columns, *J. Struct. Eng. (ASCE)*, **120** (10), 2913–2934, 1994.

[37] B.A. Izzuddin, A.A.F.M. Siyam, D.L. Smith, An efficient beam–column formulation for 3D reinforced concrete frames, *Comput. Struct.*, **80** (7–8), 659–676, 2002.

[38] C.G. Karayannis, B.A. Izzudin, A.S. Elnashai, Application of adaptive analysis to reinforced concrete frames, *J. Struct. Eng. (ASCE)*, **120** (10), 2934–2957, 1994.

[39] B.A. Izzudin, ADAPTIC User Manual, Dept. of Civil and Environmental Engineering, Revision January 2012.

[40] S. Caddemi, I. Caliò, F. Cannizzaro, Closed-form solutions for stepped Timoshenko beams with internal singularities and along-axis external supports, *Archive of Applied Mechanics*, **83** (4), 559-577, 2013.

[41] S. Caddemi, I. Caliò, F. Cannizzaro, D. Rapicavoli, "A novel beam finite element with singularities for the dynamic analysis of discontinuous frames", *Archive of Applied Mechanics*, **83** (10), 1451-1468, 2013.

[42] Ceresa, P., L. Petrini, and R. Pinho, Flexure-shear fiber beam-column elements for modeling frame structures under seismic loading—state of the art, *Journal of Earthquake Engineering*, **11** (S1), 46–88, 2007.

[43] Kagermanov, A. and P. Ceresa, Fiber-section model with an exact shear strain profile for two-dimensional rc frame structures, *J. of Struct. Eng.*, **143** (10), 04017132, 2017.

[44] F. J. Vecchio and M. P. Collins, The modified compression-field theory for reinforced concrete elements subjected to shear, *J. Proc.*, **83**, 219–231, 1986.

[45] B. Biondi, S. Caddemi, Euler-Bernoulli beams with multiple singularities in the flexural stiffness, *European Journal of Mechanics A/Solids*, **26** (5), 789-809, 2007.

[46] B. Stock , M. Halilovic, Analytical solutions in elasto-plastic bending of beams with rectangular cross section, *Appl. Math. Mod.*, **33**, 1749–1760, 2009.

[47] H.J. Bremermann, L.J. Durand III, On analytic continuation, multiplication, and Fourier transformations of Schwartz distributions, *J. Mathematical Physics*, **2**, 240–257, 1961.

[48] J.F. Colombeau, New Generalized Functions and Multiplication of Distribution. North-Holland, Amsterdam, 1984.

[49] I. Calio`, F. Cannizzaro, M. Marletta, B. Panto`, 3DMacro: A 3D Computer Program for the Seismic Assessment of Masonry Buildings. Gruppo Sismica s.r.l, Catania, 2012.

[50] I. Caliò, M. Marletta, B. Pantò, A new discrete element model for the evaluation of the seismic behaviour of unreinforced masonry buildings, *Eng. Struc.*,**40**, 327-338, 2012.

[51] B. Pantò, F. Cannizzaro, I. Caliò, P.B. Lourenço, Numerical and experimental validation of a 3D macro-model for the in-plane and out-of-plane behavior of unreinforced masonry walls, *International Journal of Architectural Heritage*,**11** (7), 946-964, 2017.

[52] HiStrA - historical structures analysis, computer program for modelling historical and monumental masonry buildings, Gruppo Sismica s.r.l., Catania, Italy (www.grupposismica.it).